Precambrian Research 411 (2024) 107529

Contents lists available at ScienceDirect

Precambrian Research

journal homepage: www.elsevier.com/locate/precamres

New perspectives on the tectonic evolution of the eastern Paraguay Belt revealed through zircon U-Pb-Hf-O systematics of the inner units

Gabriella Labate Frugis [a,*], Mario da Costa Campos Neto [a], Alice Westin [a], Christopher Mark Fanning [b]

[a] Instituto de Geociências, USP, São Paulo 05508-080, Brazil
[b] Research School of Earth Sciences, ANU, Acton ACT 0200, Australia

ARTICLE INFO

Keywords:
Western Gondwana
Paraguay Belt
Tectonic evolution
Sedimentary provenance
U-Pb-Hf-O isotopes

ABSTRACT

The Paraguay Belt and Brasília Orogen, the western and eastern segments of the Tocantins Province, respectively, recorded the interactions among the Amazonian, São Francisco-Congo Craton, and Paranapanema Block during the amalgamation of Western Gondwana. The Paraguay Belt joins the Brasília Orogen in the Transbrasiliano Lineament, which separates metasedimentary rocks to the west from metavolcano-sedimentary rocks to the east. This study focuses on four geological units cropping out in Brazil, between the Mato Grosso State southeastern region and the Goiás State western region: the Nova Xavantina Metavolcano-sedimentary Sequence (NXS), the Cuiabá Group (CG), the Barra do Garças-Coxim Unit (BGCU), a newly identified register of foreland sedimentation, and the Bom Jardim de Goiás Metavolcano-sedimentary Sequence (BJGS). Whole-rock elemental geochemistry and Nd-Sr isotopes, along with zircon U-Pb-Hf-O systematics, provide insights into the evolution of this domain.

Metavolcanic rocks from the NXS suggest that it represents a back-arc extensional tectonic environment with oceanic spreading (zircon age of ca. 710 Ma with $\delta^{18}O$ of 4.8 ‰ and chondritic $\varepsilon Hf_{(t)}$ formed along the southeastern edge of the Amazonian Craton. Metarenites preserve bimodal sources of ca. 0.85 Ga and ca. 1.90 Ga, while lithic metarenites exhibit Mesoproterozoic zircon grains suggesting sources from both the Amazonian Craton and the Paranapanema Block. The maximum depositional age of the lithic metarenites is ca. 715 Ma, coinciding with the age of the volcanic peak. The CG is interpreted as passive margin deposits through the erosion of depleted Mesoproterozoic (1.50–1.45 Ga and 1.23–1.17 Ga) and more evolved Paleoproterozoic (1.97–1.77 Ga) rocks from the Amazonian Craton.

Metasedimentary rocks from the BGCU present age peaks of 800–600 Ma, recording the input of juvenile material into the basin as revealed by zircon grains of ca. 716 Ma and ca. 810 Ma with $\delta^{18}O$ of 4.7–4.8 ‰ and $\varepsilon Hf_{(t)}$ of + 7. These findings indicate Goiás Magmatic Arc juvenile sources and disclose the evolution of the unit towards a continental arc, as suggested by more evolved zircon grains younger than ca. 700 Ma. Gneisses of ca. 690–655 Ma occur as basement rocks of the BGCU and suggest prolongation of the Goiás Magmatic Arc westward within the Transbrasiliano corridor.

1. Introduction

The Western Gondwana formation involved the diachronous assembly of continents of different sizes during the late Neoproterozoic to Cambrian. Although the geological evolution of many of these continents is well-understood, much remains unknown. This lack of knowledge is primarily due to the thick Phanerozoic deposits that cover the Proterozoic basements, making it difficult to study their geological histories. However, the extensive orogenic scars found in these regions provide valuable information on plate motion and continental interactions. By studying the characteristics of these orogens, researchers can indirectly infer the timing and nature of the interactions between continents and gain insights into the age and composition of the underlying basement.

At least nine cratons (Fig. 1A) were involved in long-term tectonic processes during the formation of Western Gondwana (Schmitt et al.,

* Corresponding author at: Rua do Lago 562, Cidade Universitária, 05508-080 São Paulo, Brazil.
E-mail address: gabriella.frugis@alumni.usp.br (G. Labate Frugis).

https://doi.org/10.1016/j.precamres.2024.107529
Received 22 August 2023; Received in revised form 28 June 2024; Accepted 19 July 2024
Available online 31 July 2024

2021). The São Francisco Craton and Paranapanema Block, in particular, exhibit deep keels of lithospheric mantle, contributing to their sustained stability over time (VanDecar et al., 1995; Julià et al., 2008; Rocha et al., 2011, 2019a, 2019b). The scarcity of reliable paleomagnetic data has led to uncertainties and different proposals regarding the movement of these crustal blocks during the Neoproterozoic.

Paleomagnetic data combined with geological observations indicate that the Amazonian paleoplate was linked to Laurentia during the late Tonian to Cryogenian, which was separated from both the São Francisco-Congo and Río de la Plata continents (Cordani et al., 2003; Tohver et al., 2006; D'Agrella-Filho and Cordani, 2017; Rapalini, 2018). A vast ocean likely existed between them, the Goiás-Pharusian Ocean (Cordani et al., 2013b; D'Agrella-Filho and Cordani, 2017). The Paranapanema Block is not exposed, therefore, no paleomagnetic data are available. The limited paleomagnetic data contrast with the extensive geological record from the adjacent orogens which are used to constrain the tectono-geographic evolution of this area.

The studied area encompasses part of the Tocantins Province, including the lower Cambrian low-grade metamorphic rocks of the Paraguay Belt (Almeida, 1984; Alvarenga and Trompette, 1993; Boggiani and Alvarenga, 2004). It is separated from the Tonian-Cryogenian orthogneisses and metavolcano-sedimentary rocks of the Goiás Magmatic Arc (Brasília Orogen) by the Transbrasiliano Lineament (Cordani et al., 2013a; Curto et al., 2014; Pimentel, 2016; Fuck et al., 2017; Valeriano, 2017; and references therein), which, in this region, is buried by the Phanerozoic cover. However, the lineament is marked by a step in lithospheric thickness, with a thicker lithosphere to the east (Azevedo et al., 2015; Rocha et al., 2019a).

The Cambrian magmatic and metamorphic ages of the Paraguay Belt (Geraldes et al., 2008; Godoy et al., 2010; Piacentini et al., 2013; Tohver et al., 2010, 2012, 2016) overlap with those of the Pampean Orogeny to the south (Escayola et al., 2007; Schwartz et al., 2008; Dahlquist et al., 2016; López de Luchi et al., 2018). They suggest a coeval suture zone between the Eastern Sierras Pampeanas (Ramos et al., 2010) and Rio

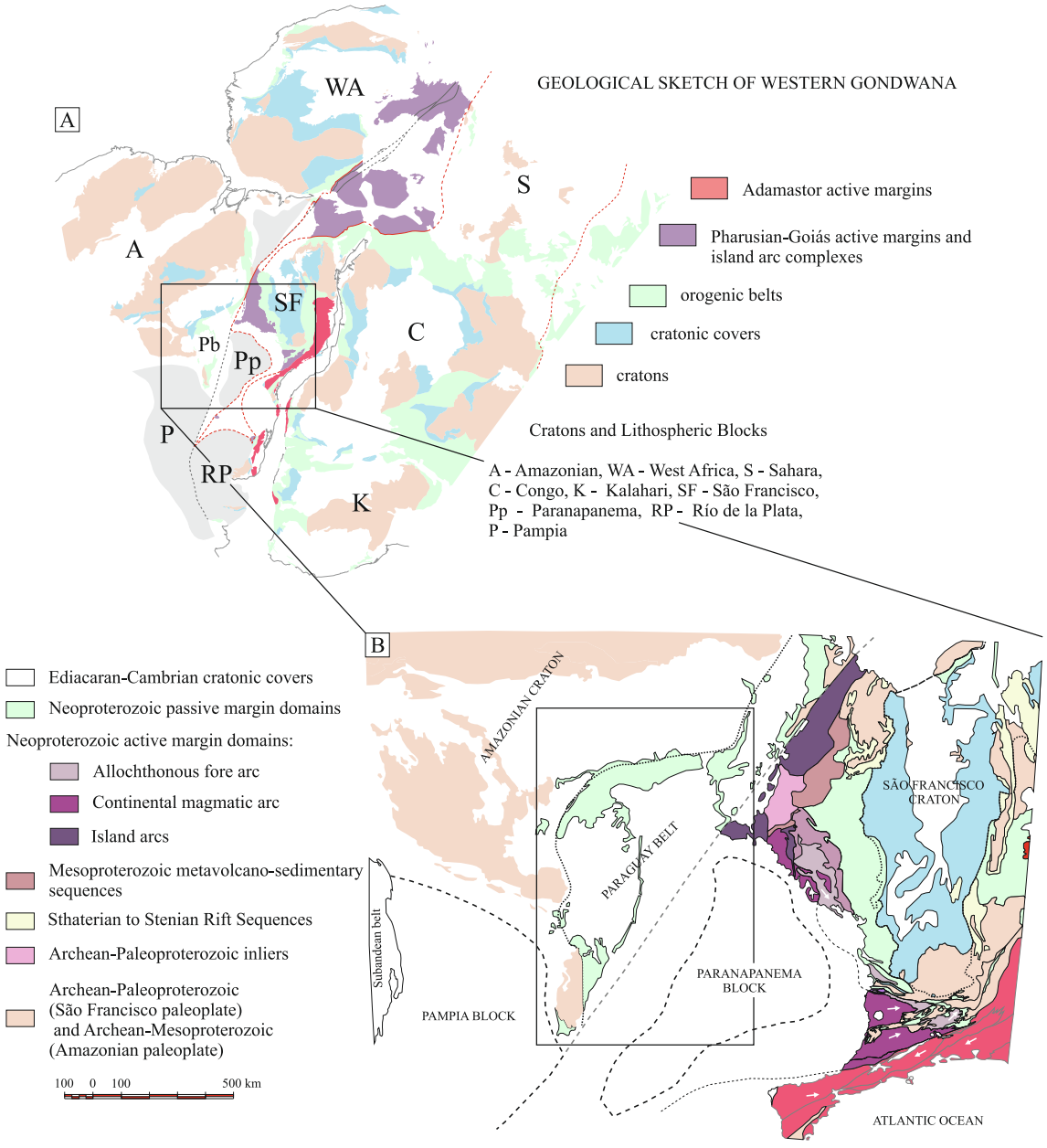

Fig. 1. (A) Partial view of Western Gondwana (compiled and modified after Schmitt et al., 2018 and references therein); (B) Simplified tectonic map of central-southeast South America (modified from the Tectonic Map of South America, Cordani et al., 2016).

Apa-Amazonian cratons, and the western Río de la Plata Craton and Paranapanema Block (priorly sutured across the Paraguari Belt; Leite et al., 2018). The understanding of the Transbrasiliano Lineament as being an element of the suture zone west of the Paranapanema-Río de la Plata cratons (Curto et al., 2014; Ganade de Araujo et al., 2014), supports ocean closure through collisional processes between these continental masses (Tohver et al., 2012; McGee et al., 2018). This ocean, named the Clymene Ocean (Trindade et al., 2006), has been controversial, as its closure in the Ediacaran would represent the amalgamation of the São Franscisco-Congo with the Amazonian Craton, and the

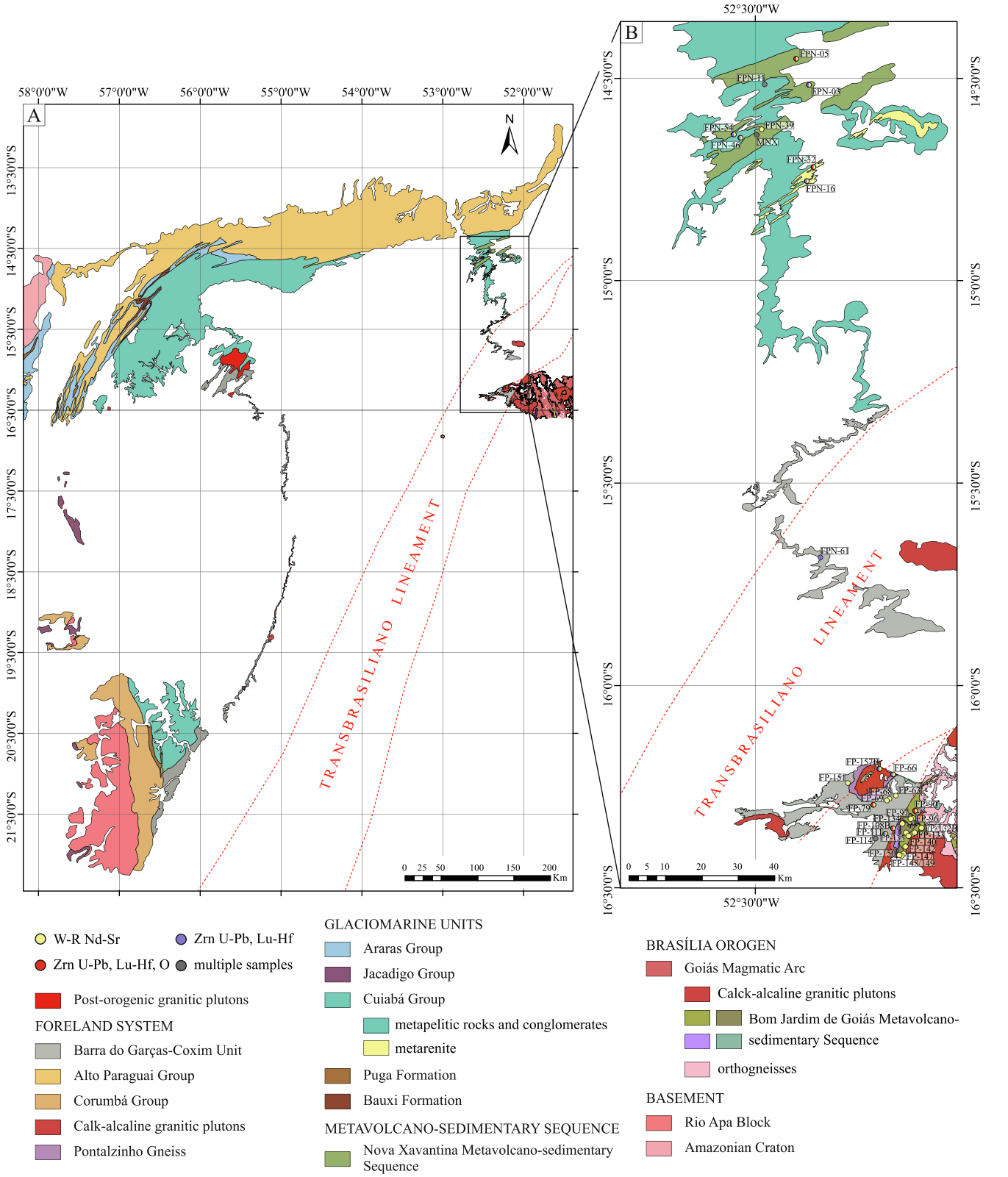

Fig. 2. (A) Geological map of the Paraguay Belt. The studied area is highlighted; (B) Geological map of the studied area with location of the main analyzed samples. Zrn = zircon; W-R = whole-rock.

timing of this closure with respect to the separation of the Amazonian paleoplate from Laurentia governs the existence of the putative continent Pannotia (Dalziel, 1997; Cordani et al., 2013b; Ganade de Araujo et al., 2014). This issue will be carefully addressed when discussing the eastern segment of the Paraguay Belt.

Here we integrate data from whole-rock elemental and isotopic geochemistry with zircon U-Pb-Hf-O data from metasedimentary, metavolcanic, metavolcaniclastic and gneissic rocks located in the transitional zone between the Eastern Paraguay Belt and the Western Brasília Orogen, in the Central-West region of Brazil (Fig. 1B). In combination with the available data, we propose a new interpretation of the tectonic environment and final stages of Western Gondwana assembly through provenance and volcanic evolution investigations.

2. Geological setting

The Paraguay Belt is a fold-and-thrust belt developed among the Amazonian, Rio Apa, and Paranapanema cratonic margins and comprises sedimentary, volcano-sedimentary, and low-grade metamorphic rocks of Tonian-Cambrian age. The curved shape of the belt, convex towards the Amazonian Craton, is roughly N-S-oriented in the southern and eastern segments and E-W-oriented in the northern segment, set apart by Phanerozoic cover rocks (Fig. 1B).

The sedimentary sequences of the southern segment overlie the Amazonian-Rio Apa cratons and comprise a rift-drift series of the Jacadigo and Corumbá groups (Almeida, 1945; Boggiani and Coimbra, 1996; Campanha et al., 2011; Freitas et al., 2011; Angerer et al., 2016; McGee et al., 2018) (Fig. 2A). The Jacadigo Group recorded two Cryogenian events of glacioeustatic incision and transgression (Sturtian and Marinoan cryochrons), culminating in massive Fe and Mn deposits (Freitas et al., 2021) containing rare earth elements and yttrium related to an open ocean under oxic atmosphere/hydrosphere conditions (Viehmann et al., 2016). The maximum depositional age varies from ca. 1.3 Ga in the basal units to ca. 690 Ma in the upper ones (Babinski et al., 2013; Frei et al., 2017; Freitas et al., 2021). This group partially corresponds to the basal clastic deposits of the Corumbá Group, which includes Marinoan diamictites (McGee et al., 2018). The stromatolitic dolomites and phosphorites of the Bocaina Formation overlie the siliciclastic rocks and record the drifting stage of a passive continental margin (Boggiani and Alvarenga, 2004). Volcanic ash horizons at the top of the unit registered the end of the Ediacaran (ca. 555 Ma; Parry et al., 2017). The fossiliferous and bituminous limestones of the Tamengo Formation and upper-laminated calcareous siltstones of the Guaicurus Formation unconformably overlie the Bocaina Formation (Fig. 3). The volcanic tuff beds at the top of the Tamengo Formation have an age of ca. 543 Ma (Babinski et al., 2008; McGee et al., 2018), constraining the occurrence of bilaterian fossil remains to the end of the Ediacaran and the deposition of the upper fossiliferous siltstones of the Guaicurus Formation to the early Cambrian (Parry et al., 2017).

The northern E-W striking segment of the Paraguay Belt (Fig. 1B, 2A) comprises a series of glaciomarine and turbiditic sedimentary rocks interpreted to be deposited in a passive margin environment developed between the Marinoan and Gaskiers cryochrons. They form an unconformable cover to the craton in the west and progress eastward into a west-verging fold-and-thrust belt, corresponding to the Puga and Bauxi formations (Alvarenga and Saes, 1992) and the Cuiabá Group (Alvarenga and Trompette, 1988, 1992, 1993; Tokashiki and Saes, 2008; McGee et al., 2015a). Their lithostratigraphic log (Fig. 3) comprises a siliciclastic basal unit mainly composed of intermediate turbiditic layers associated with metarkoses and metadiamictites, subordinated metalimestones and hematite beds, and phyllites with lenses of calcitic and dolomitic marbles at the top. This last sequence progresses laterally, toward the west, to the Araras Group (Almeida, 1964), a proximal carbonate platform of passive margin setting. Detrital zircon grains indicate the main source provided by the Mesoproterozoic Sunsás Province of the Amazonian Craton, and a maximum depositional age of ca. 650 Ma in consonance with Pb/Pb isochron ages of ca. 630–620 Ma obtained for the cap carbonate in the cratonic domain (Babinski, 2011; Romero et al., 2012; McGee et al., 2015a, 2015b; Babinski et al., 2018). Incision surfaces and paleovalleys filled with massive diamictites, striate sandstones and outsized lonestones at the top of the Araras Group were related to isostatic rebound, glacial erosion and sea level fall during the Gaskiers Glaciation (ca. 580 Ma; Alvarenga et al., 2007; McGee et al., 2013).

The eastern segment consists of the pre-Sturtian Nova Xavantina Metavolcano-sedimentary Sequence (Pinho, 1990; Martinelli, 1998; Silva, 2007, 2018; Sousa et al., 2019) overlapped by the Cuiabá Group (Figs. 2 and 3). The lithostratigraphic section of the Nova Xavantina Sequence comprises metabasalts of T-MORB affinity associated with iron formations, carbonaceous phyllites, and metacherts of Tonian age (ca. 770–745 Ma) covered by pyroclastic felsic rocks of ca. 735 Ma, along with phyllites, metasiltstones, and metagabbro dykes of ca. 715 Ma that intruded them (Silva, 2007, 2018). Phyllites with polymictic metaconglomerates, diamictites, marbles, and immature metarenites at the top constitute the metasedimentary sequence of the Cuiabá Group. Carbonaceous black slates recovered by drilling cores at the base of the Cuiabá Group in the northern segment of the belt yielded a Re-Os sedimentation age of ca. 780 Ma (Manoel et al., 2021), suggesting prolongation of the Nova Xavantina Metavolcano-sedimentary Sequence to the west.

A collisional foreland basin system (e.g., DeCelles and Giles, 1996) frames the Paraguay Belt (Fig. 1B, 2A and 3). They conform to the western external cratonic back-bulge basin of siliciclastic rocks of the Alto Paraguay Group (Almeida, 1964; Alvarenga, 1988; McGee et al., 2015b) and the low-grade metamorphic internal zone of the eastern terrigenous-filled basins of the Barra do Garça-Coxim Unit (this study). This unit is in tectonic contact with the Goiás Magmatic Arc through the Transbrasiliano Lineament, which is locally represented by the Serra Negra dextral shear zone (Seer, 1987; Curto et al., 2014). A forebulge domain with deformed rocks from the Cuiabá and Corumbá groups occurs between these basins. Detrital zircon patterns revealed a major shift in the source area. The metamorphic and internal eastern domain of the Paraguay Belt supplied a record of heavy detrital minerals in the back-bulge basin with a maximum depositional age of ca. 540–530 Ma (Bandeira et al., 2012; McGee et al., 2015b). The Brasília Orogen and the inner domain of the belt provided the source of detrital zircon grains to the Barra do Garça-Coxim Unit between ca. 800 Ma and ca. 590–535 Ma (Pelosi, 2017; Vasconcelos, 2018; this paper).

Potassic ultramafic rocks intruded the Cuiabá Group and Puga Formation at ca. 605–575 Ma (biotite $^{40}Ar/^{39}Ar$ and zircon U-Pb ages). This ultramafic magmatism is interpreted to be related to an extensional tectonic event (Min et al., 2013; Silva, 2018).

Granitoids were found in the inner foreland unit. They registered 550–540 Ma pre- to *syn*-collisional magmatic stages, and a late- to post-collisional stage that lasted until 500 Ma (Ferreira, 2009; Godoy et al., 2010). The São Vicente granitic batholith of 518 ± 4 Ma represents the post-tectonic event (McGee et al., 2012).

Orthogneisses and supracrustal rocks of the southern Goiás Magmatic Arc of the Brasília Orogen (Arenópolis Arc; Pimentel et al., 2000) are exposed in the southeast of the Paraguay Belt. The Arenópolis Arc comprises metavolcanic-sedimentary arc-related sequences lasting from 900 to 540 Ma. They record the orogenic transition from island arc to active continental margin setting in the northeast Paranapanema Craton and the late- to post-orogenic stages with granite magmatism (Pimentel and Fuck, 1987; Pimentel et al., 1999, 2000, 2003; Laux et al., 2004; Pimentel, 2016; Carneiro et al., 2021).

The Bom Jardim de Goiás Metavolcanic-sedimentary Sequence is the eastern Tonian juvenile sequence (ca. 750 Ma; Guimarães et al., 2012) of andesitic metabasalts, including pillow lavas, metatuffs, and metavolcanic rocks with subordinate metasedimentary rocks and granitic orthogneisses (Seer and Nilson, 1985; Seer, 1987). The Serra Negra dextral shear zone, a tectonic tract of the Transbrasiliano Lineament, separates it from the inner foreland unit of the Paraguay Belt (Fig. 2A).

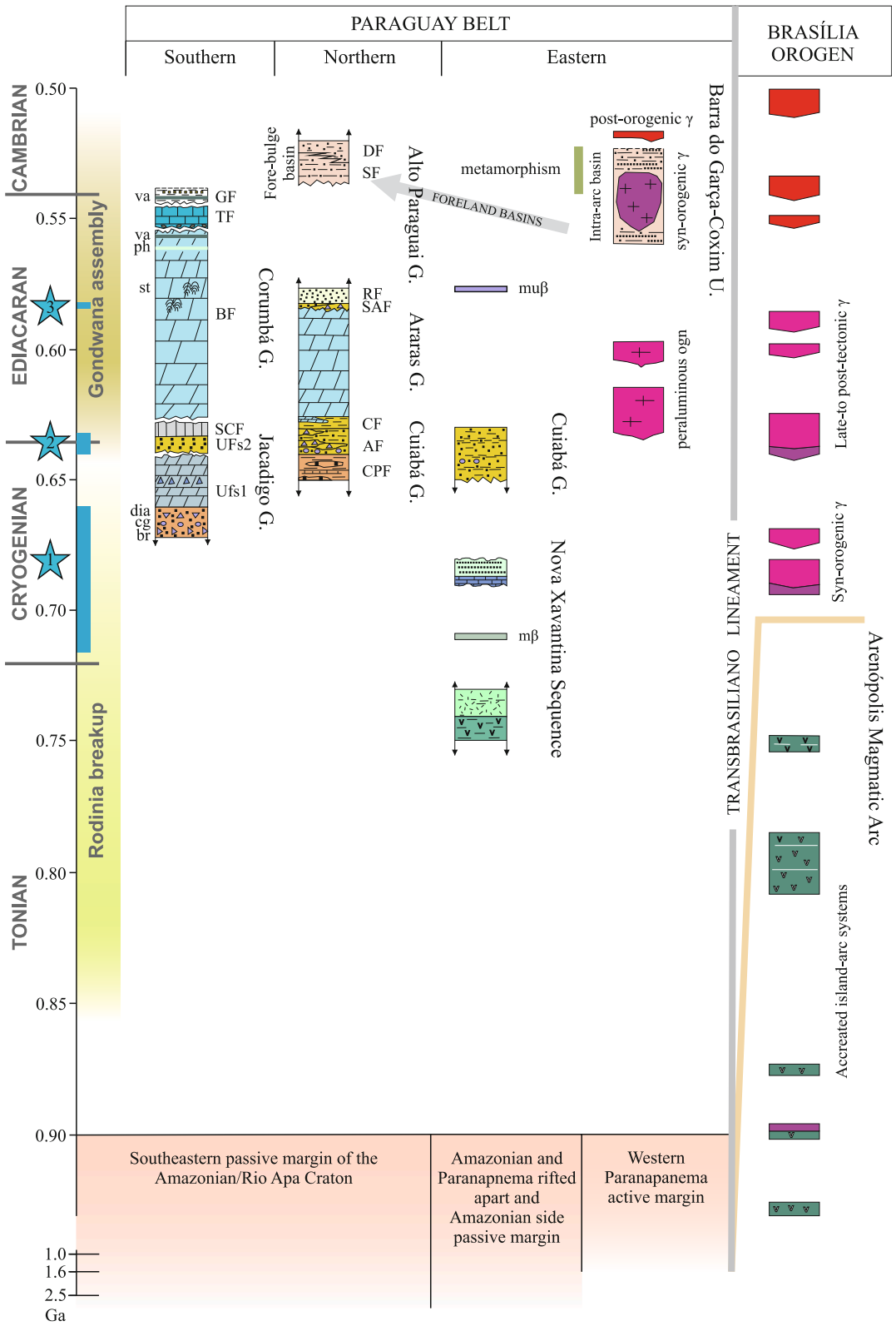

Fig. 3. Stratigraphic-tectonic log: 1 = Sturtian cryochron; 2 = Marionan cryochron; 3 = Gaskiers cryochron; va = volcanic ash; ph = phophorite layers; st = stromatolite; dia = diamictite; cg = conglomerate; br = breccia; GF = Guaicurus Fm.; TF = Tamengo Fm.; BF = Bocaina Fm.; SCF = Santa Cruz Fm.; UFs2 = Urucum Fm. sequence 2; UFS1 = Urucum Fm. sequence 1; DF = Diamantino Fm.; SF = Sepotuba Fm.; RF = Raizama Fm.; CF = Coxipó Fm.; AF = Acorizol Fm.; CPF = Campina das Pedras Fm.; muβ = metaultramafic rocks; mβ = metagabbro.

3. Materials and methods

Sixty samples were collected for whole-rock elemental geochemistry, forty-four were selected for whole-rock Sm-Nd and Rb-Sr isotopes, eighteen for U-Pb zircon geochronology, seventeen for Lu-Hf isotopes, and seven for O stable isotopes, both on zircon grains. Supplementary Material I provides a table of the analyzed samples with UTM coordinates and the type of analysis performed in each case (item I.1). It also contains the analytical procedures and details for each type of methodology (items I.2 to I.6), as well as outcrop photographs (item I.7).

The acronyms FPN and FP correspond to the Northern Paraguay Belt and Paraguay Belt, respectively, and MNX refers to samples obtained from boreholes drilled by the NX Gold Mining Company in the Nova Xavantina City.

3.1. Whole-rock elemental and isotopic analyses

The preparation of the samples analyzed for whole-rock geochemistry involved cleaning, crushing in a hydraulic press, quartering, and separation of 100 g for milling in a planetary-type agate ball mill. The procedures were conducted at the Sample Treatment Laboratory of the NAP Geoanalítica of the Geosciences Institute of the University of São Paulo (IGc-USP) (further details are provided in Supplementary Material I, items I.2 and I.3).

3.2. Zircon U-Pb, Lu-Hf and O systematics

The samples were prepared at the Separation and Preparation Laboratory of the Geochronology and Isotopic Geochemistry Research Center (CPGeo), IGc-USP, following well-established protocols for heavy mineral separation. The process included sieving to separate fractions between 100 and 250 μm, heavy material concentration using a Wilfley Table, a hand magnet, a Frantz isodynamic separator, and heavy liquids (bromoform and methylene iodide). Subsequent manual selection of zircon crystals under a magnifying glass was preceded by mounting and polishing of the grains in epoxy resin discs. Cathodoluminescence images were obtained using a FEI Quanta 250 VPS electron microscope at the Scanning Electron Microscopy Laboratory of the CPGeo. These images served as guides for the in situ U-Pb analyses.

The U-Pb analyses were performed using a Thermo Scientific NEPTUNE LA-MC-ICP-MS with a 193 nm Excimer laser (Teledyne) at the LA-MC-ICP-MS Laboratory of the CPGeo (more details are provided in Supplementary Materials I, item I.4). Analyses with discordances higher than 10 % and common Pb higher than 5 % of the total Pb (i.e., radiogenic + common Pb) were discarded. The results were plotted using IsoplotR (Vermeesch, 2018) for Kernel density estimation. The maximum depositional ages (MDA) were estimated using Density Plotter software (Vermeesch, 2012) and the minimum age model tool. Diagrams were calculated considering the 1500 Ma cutoff age for switching from $^{206}Pb/^{238}U$ dates (<1500 Ma) to $^{207}Pb/^{206}Pb$ dates (>1500 Ma), following the procedures described by Puetz et al. (2021).

Lu-Hf analyses were performed on selected zircon grains of both igneous and detrital origins, previously dated by LA-MC-ICP-MS U-Pb at the CPGeo. The LA-MC-ICP-MS equipment used to acquire the U-Pb data was the same as that used for the Lu-Hf analyses (more details are provided in Supplementary Materials I, item I.5).

Oxygen isotope analyses were performed on seven samples at the Research School of Earth Sciences of the Australian National University (ANU) using a SHRIMP II equipment. The analytical procedures used in this study have been described by Ickrt et al. (2008) (more details are provided in Supplementary Materials I, item I.6).

4. Results

Below, we present succinct petrographic features of the analyzed samples; for more details, see item II.1 for Nova Xavantina Sequence samples, item II.2 for Bom Jardim de Goiás Sequence samples, item II.3 for Cuiabá Group samples, and item II.4 for Barra do Garças-Coxim Unit samples in Supplementary Material II. The whole-rock XRF, ICP, and Sr-Nd data are shown in items III.1, III.2, and III.3, respectively, of Supplementary Material III. The zircon U-Pb, Lu-Hf, and O data can be found in items III.4, III.5, and III.6, respectively, of Supplementary Material III.

4.1. Petrography and geochemistry

4.1.1. Nova Xavantina Metavolcano-sedimentary Sequence

The metapsammitic rocks are reddish metarenites with fine-grained matrix and bimodal quartz grain size. Granoblastic texture is prevalent and dynamic recrystallization textures, such as bulging and subgrain rotation, are common. Feldspar makes up less than 5 % and is easily recognized through alteration textures such as saussuritization. The reddish color is due to the presence of iron oxides, which occur as thin crystals in the matrix. Clasts of quartzites, metacherts, and sericite-rich rocks are also present.

The metapelitic rock is a fine-grained chlorite-quartz-muscovite schist with muscovite-graphite rich bands. These layers are often rich in quartz, white mica, chlorite, graphite, and sericite. Graphite marks thin folded lenses with disrupted hinges transposed by the main foliation. These lenses correspond to the original sedimentary stratification. White mica forms sigma-type kinematic indicators along microcrystalline quartz-rich bands.

The metacalcarenite rock was also analyzed and presents granulometric stratification marked by a thin subidioblastic carbonatic matrix with sericite and quartz. The framework is composed of subangulose-oriented to angulose-oriented granules of plagioclase, quartz, and scarce muscovite. Chlorite-sericite-rich rocks occur as lithic fragments with sub-rounded to elongated shapes. Idioblastic carbonate grains, ovoid carbonate intraclasts, and ooids are also observed.

One of the lithic metarenites is a medium-grained welded rock with strong carbonatization and slight deformation, although the original structures are preserved. Carbonate substituted the rock matrix and varies from subidiomorphic to xenomorphic. Clasts and lapilli with sub-rounded to ovoid shapes are common. The other exhibits more pervasive hydrothermal alteration with the presence of a fine-grained sericitized and chloritized matrix and no longer preserves its original mineralogy or structures.

In the classification diagram (Fig. 4A), metarenites are classified as quartz arenites, metapelitic rocks are chemically compatible with mudstones and wakes, whereas the lithic metarenite is classified as Fe-rich shale, although the thin section suggests the presence of lithic fragments. The REE contents of the lithotypes are variable, with all the analyzed samples having a strong fractionation of REE (La_N/Yb_N = 3.24–25.39) and LREE (La_N/Sm_N = 1.13–6.50), and lower fractionation of HREE (Gd_N/Yb_N = 0.99–3.00) (Fig. 4B). The samples also have negative Eu anomalies from 0.59 to 0.91, with one outlier with 1.02 (Fig. 4B). The REE pattern of the lithic metarenites present La_N/Yb_N from 5.38 to 6.82, La_N/Sm_N from 1.49 to 2.14, and Gd_N/Yb_N from 2.58 to 3.01 (Fig. 5D).

Major and trace elements tectonic discrimination diagrams suggest that the metapsammitic rocks protoliths were derived mainly from mafic igneous rocks (F1 = -9.08 and F2 = -4.89) related to depleted mantle (Th = 1.06 and Th/U = 1.23) and upper crust sources (Th = 0.99 and Th/U = 5.67) (Fig. 4D, E). The source area of the metapelites was mainly composed of quartzose sedimentary units (F1 = 3.31–4.82 and F2 = 1.26–4.72) related to the upper crust (Th = 17.89 and Th/U = 3.99) and depleted mantle sources (Th = 0.49 and Th/U = 1.58). The high ratios of Th/Sc and Zr/Sc of the metapsammitic rocks suggest that these rocks were strongly recycled (Th/Sc = 0.81–8.00 and Zr/Sc = 107.33–117.07), with exception of the lithic metarenite (Th/Sc = 0.12 and Zr/Sc = 4.60), while the metapelites tend to have smaller ratios (Th/Sc = 0.04–1.47 and Zr/Sc = 3.05–15.79), which suggests a source area composed of intermediate igneous rocks with an important upper

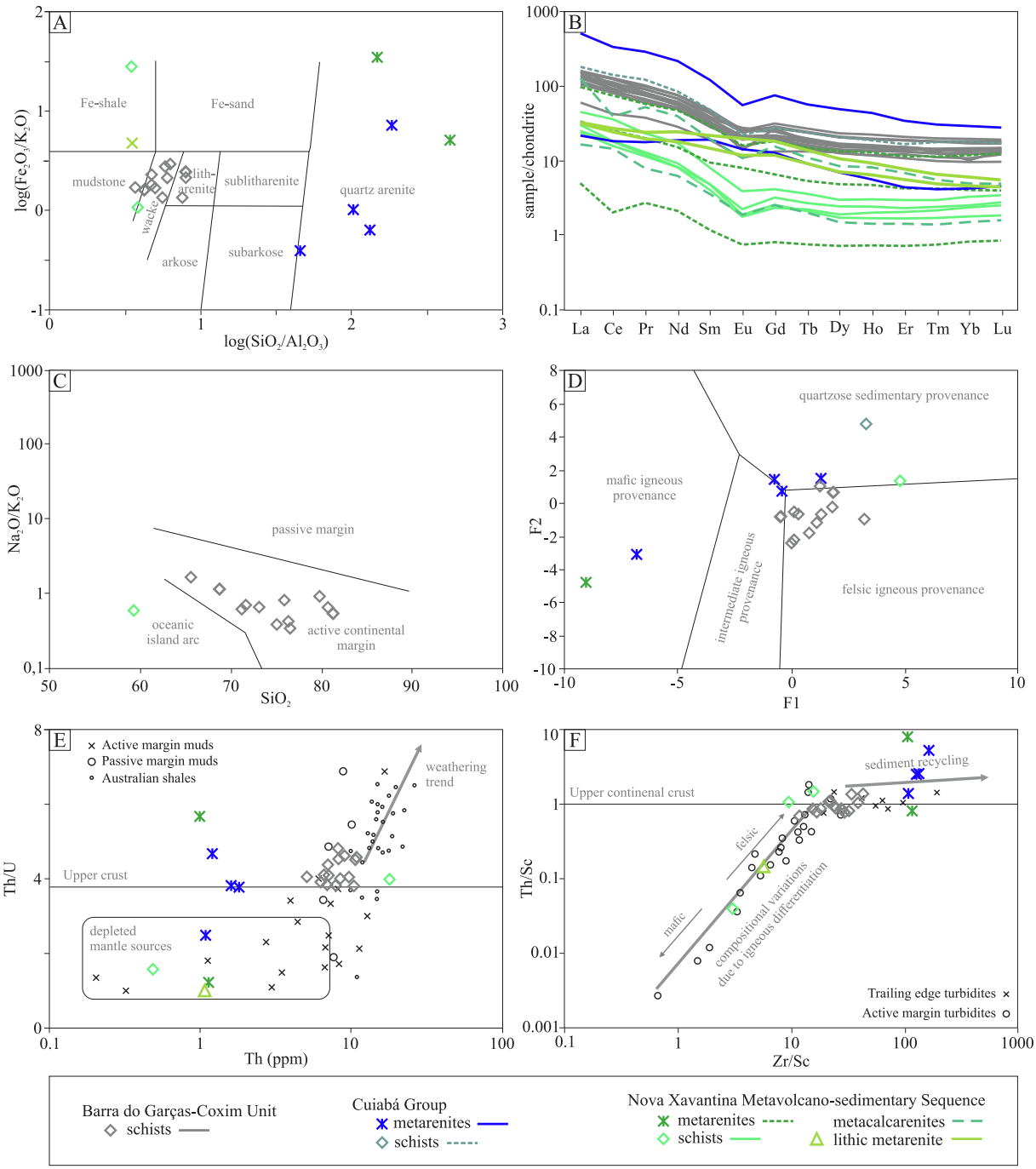

Fig. 4. Diagrams for metasedimentary rocks. (A) Geochemical classification of metasedimentary rocks (Herron, 1988); (B) REE spider diagram of metasedimentary rocks; (C) Na_2O/K_2O versus SiO_2 diagram (Roser and Korsch, 1986); (D) provenance diagrams applying discriminant function analysis (Roser and Korsch, 1988: F1 = $30.638TiO_2/Al_2O_3 - 12.541Fe_2O_3(total)/Al_2O_3 + 7.329MgO/Al_2O_3 + 12.031Na_2O/Al_2O_3 + 35.402K_2O/Al_2O_3 - 6.382$; F2 = $56.5TiO_2/Al_2O_3 - 10.879Fe_2O_3(total)/Al_2O_3 + 30.875MgO/Al_2O_3 - 5.404Na_2O/Al_2O_3 + 11.112K_2O/Al_2O_3 - 3.89$); (E) Th/U versus Th diagram (McLennan et al., 1993); (F) Th/Sc versus Zr/Sc diagram (McLennan et al., 1993).

continental crust component (Fig. 4F). An active tectonic environment is suggested (Fig. 4C).

The analyzed metavolcanic rocks have mineralogical and textural evidence of hydrothermal alteration. The lithologies vary between metavolcanic rock with metamorphic foliation, and a crystalline matrix, amygdaloidal metavolcanic rock with crystalline chloritized matrix, and volcanic breccia with crystalline chloritized matrix. Elongated and deformed amygdale are rare but occur disperse and seem to be filled with microcrystalline quartz and chlorite. Dark pleochroic chlorite substitutes previous minerals being seen as skeletal pseudomorphs.

The major elements of the unaltered metavolcanic rocks are chemically compatible with both the calc-alkaline and tholeiitic series (Fig. 5A). The most immobile trace elements also suggest a mafic to intermediate composition for the metavolcanic rocks (Fig. 5B). The metavolcanic rocks are richer in LREE than in HREE, with high fractionation of REE (La_N/Yb_N = 0.50–5.62) and HREE (Gd_N/Yb_N = 2.67–3.06), and lower fractionation of LREE (La_N/Sm_N = 1.24–2.27) (Fig. 5C). The Eu and Ce anomalies are slightly negative to non-existent (Eu/Eu* = 0.89–1.00 and Ce/Ce* = 0.98–0.99). Tectonic discrimination diagrams suggest that the metavolcanic rocks have E-MORB, within-

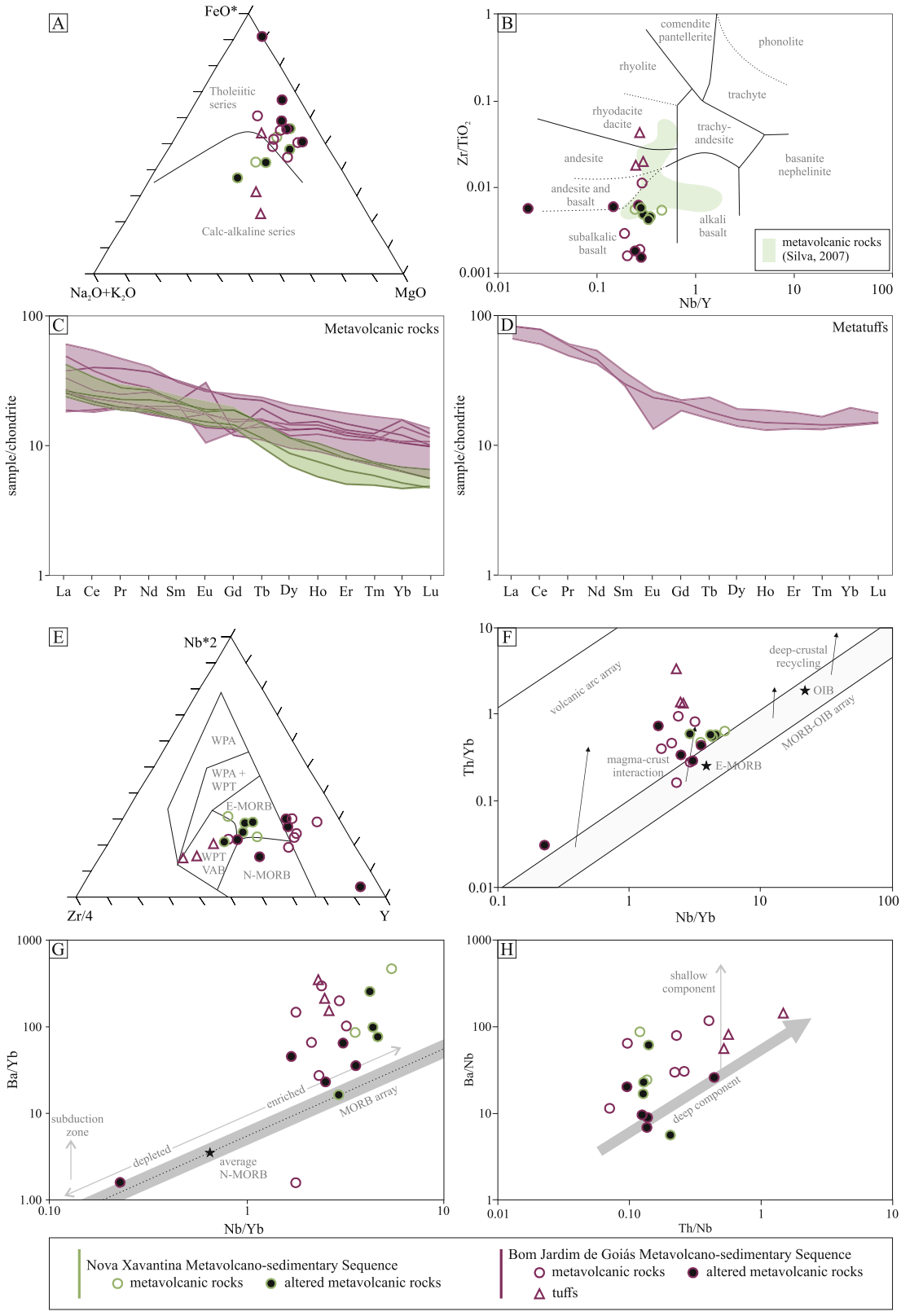

Fig. 5. Diagrams for metavolcanic and metavolcaniclastic rocks. (A) AFM diagram; (B) Nb/Y versus Zr/TiO_2; REE spider diagrams of (C) volcanic rocks and (D) tuffs; (E) Nb*2 – Zr/4 – Y diagram (WPA: within-plate alkali basalt, WPT: within-plate tholeiites, VAB: volcanic arc basalts, MORB: mid-ocean ridge basalts; Meschede, 1986); (F) Th/Yb versus Nb/Yb diagram (Pearce, 2008); (G) Ba/Yb versus Nb/Yb diagram (Pearce and Stern, 2006); (H) Ba/Nb versus Th/Nb diagram (Pearce and Stern, 2006).

plate tholeiites, or volcanic arc basalt affinities (Fig. 5E) and were differentiated from an E-MORB parental magma (Fig. 5F) with subordinate magma-crust interaction (Fig. 5G) and shallow component influence (Fig. 5H).

4.1.2. Bom Jardim de Goiás Metavolcano-sedimentary Sequence

The main analyzed metavolcanic rocks are titanite-chlorite-epidote-actinolite mylonitic schists, tremolite/actinolite-chlorite schists with epidote, (quartz-plagioclase)-actinolite schists with epidote and titanite, and andesites/dacites. The samples are fine-grained rocks and some are cross-cut by carbonate-filled veins. Actinolite and epidote can occur as sub-rounded porphyroblasts with tails, forming sigma- and delta-type kinematic indicators. Well-formed rectangular plagioclase crystals are preserved in some samples. Metavolcaniclastic rocks are classified as crystal tuffs with visible crystal fragments.

The metavolcanic rocks are compatible with the tholeiitic series (Fig. 5A) and are chemically classified as subalkaline basalt, andesite and basalt (Fig. 5B). The tuff samples are compatible with the calc-alkaline series (Fig. 5A) and were classified as chemically similar to subalkalic basalts (Fig. 5B). The REE contents of the metavolcanic rocks (ΣREE = 43.44–95.84) are slightly lower than the tuffs content (ΣREE = 98.11–123.27) (Fig. 5C, D). The metavolcanic rocks also exhibit a weaker fractionation of REE (La_N/Yb_N = 1.73–4.07), LREE (La_N/Sm_N = 0.96–2.37), and similar HREE (Gd_N/Yb_N = 0.82–2.68) than the tuffs (La_N/Yb_N = 4.22–5.85; La_N/Sm_N = 2.23–2.91; Gd_N/Yb_N = 1.14–1.48). The metavolcanic rocks present mainly positive Eu anomalies (1.00–1.83), with few exceptions (0.65–0.95), while the tuffs present all negative Eu anomalies (0.58–0.92).

Trace elements used to distinguish the parental magma and tectonic setting suggest a volcanic arc basalt composition close to E-MORB character for the samples (Fig. 5E), probably with magma-crust interaction (Fig. 5F) from enriched MORB closer to the subduction zone

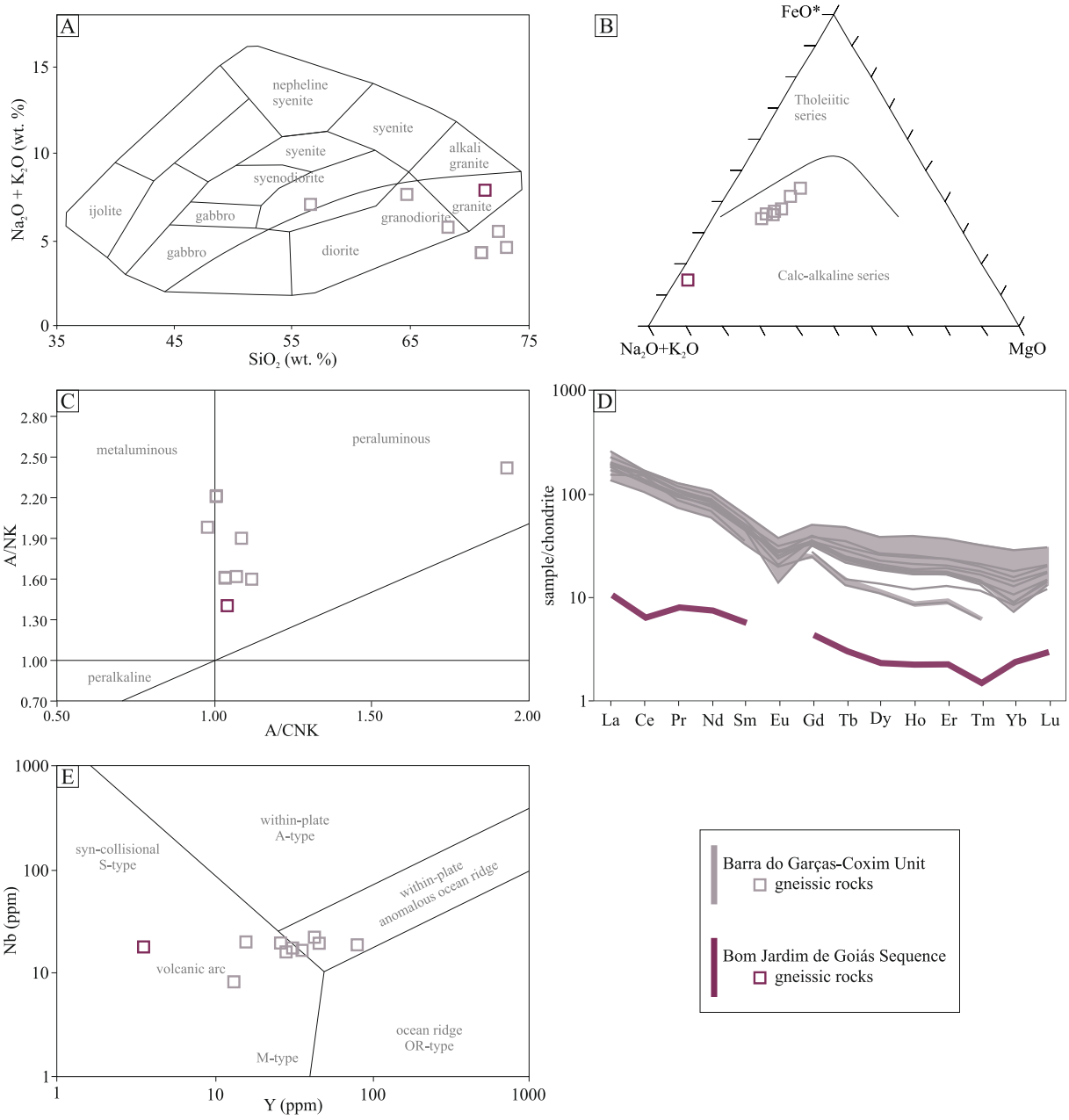

Fig. 6. Diagrams for gneissic rocks. (A) $Na_2O + K_2O$ versus SiO_2 classification diagram; (B) AFM diagram (Irvine and Baragar, 1971); (C) REE spider diagrams of orthogneiss; (D) A/NK versus A/CNK plot (Maniar and Piccoli, 1989); (E) Nb versus Y diagram (Pearce et al., 1984).

(Fig. 5G) and related to shallow depth components (Fig. 5H).

The analyzed gneiss is a medium-fine-grained layered titanite-epidote-muscovite-biotite-plagioclase-quartz granite gneiss with alternating granoblastic and lepidogranoblastic bands. The granoblastic bands are composed of quartz and plagioclase, which may have preserved their original igneous features. In some cases, sericite can partially or completely substitute plagioclase crystals, and in a few cases, xenoblastic carbonates may occur. The thinner and discontinuous biotite-rich lepidoblastic bands display accessory phases of muscovite, epidote, plagioclase, apatite, and titanite.

The sample were chemically classified as granite (SiO_2 = 71.27 %; $Na_2O + K_2O$ = 7.84 %) (Fig. 6A) and is chemically compatible with the calc-alkaline series (A = 82.28, F = 14.52, M = 3.21) (Fig. 6B) with a peraluminous character (A/CNK = 1.04; A/NK = 1.40) (Fig. 6C). It is is strongly depleted in REE content compared to the orthogneisses of the Foreland Unit (ΣREE = 13.94), with La_N/Yb_N = 4.45, La_N/Sm_N = 1.87, and Gd_N/Yb_N = 1.83, and a slightly negative Ce anomaly of 0.69 (Fig. 6D). Trace element tectonic discrimination diagrams suggest that the igneous protolith was generated in a volcanic arc environment (Fig. 6E).

4.1.3. Cuiabá Group

Four fine-grained, well-selected metarenites were analyzed. In general, quartz crystals exhibit an oriented wavy extinction, and in elongated grains, dynamic recrystallization occurs through bulging grain boundaries, forming microcrystalline domains. The former plagioclase grains may have undergone sericitic alteration. There are clasts of chert, ferruginous chert, and quartzites, as well as detrital muscovite, tourmaline, and epidote.

The analyzed metapelitic rock (slate) is compound by small-sized white micarich matrix with graphite and probably chlorite. It is matrix-supported although exhibit high volume of granules. It preserves a sedimentary compositional banding marked by matrix-rich and granules-rich bands. In the matrix-rich portions, crenulation cleavage occurs oblique to the sedimentary banding. Framework is composed mainly by quartz with minor volume of twinned plagioclase.

In the classification diagram (Fig. 4A), all metarenites were classified as quartz arenites. The REE content in the metasedimentary rocks are variable and tend to be higher than that in the metasedimentary rocks of the Nova Xavantina Sequence (Fig. 4B). They all present Eu anomalies (0.54–0.68) and flat patterns in the HREE (Gd_N/Yb_N = 0.99–1.43) (Fig. 4B). These rocks predominantly present quartzose sedimentary sources within the upper continental crust with a few mafic igneous influences (Fig. 4D, E, F). The slate sample plots outside in some diagrams.

4.1.4. Barra do Garças-Coxim Unit

Four metapelites were analyzed from the Barra do Garças-Coxim Unit, one being a quartz-chlorite-muscovite schist finely banded with quartz-rich tight-folded millimetric bands. Microlithons preserves the former foliation, whereas the main schistosity is folded. An epidote-biotite-chlorite-muscovite-plagioclase-quartz banded schist with marked intercalation between the granolepidoblastic and lepidogranoblastic bands also occurs. Micaceous minerals define the crenulated schistosity, and quartz and plagioclase occur as elongated crystals oriented parallel to the foliation. The other sample is a fine-grained plagioclase-biotite-muscovite-quartz mylonitic schist with tourmaline. The rock exhibits mylonitic schistosity, in which the micaceous minerals mark an anastomosed foliation in the S-C pairs. Finally, a fine-grained plagioclase-biotite-muscovite-quartz mylonitic schist with mylonitic schistosity was also analyzed, where the micaceous minerals mark the anastomosed S-C pairs. Transitional banding between granoblastic and lepidoblastic bands is visible, and agglomerates of mica tend to form sigma-like shapes in mica fishes.

In the classification diagram (Fig. 4A), the schists are chemically compatible with mudstone, wacke, and lithic arenite. The samples have similar REE contents, with low fractionation of REE (La_N/Yb_N = 4.05–15.78), LREE (La_N/Sm_N = 3.15–4.62) and HREE (Gd_N/Yb_N = 0.90–2.64) and slightly negative Eu anomalies between 0.47 and 0.92 (Fig. 4B). Major elements suggest an active continental margin origin (SiO_2 = 65.61–81.32 and K_2O/Na_2O = 0.35–1.69) with felsic igneous provenance (F1 = -0.45–3.24 and F2 = -2.52–0.95) (Fig. 4C, D). Trace element contents indicate that the protoliths of these rocks were derivated from upper continental crust sources (Th = 5.07–10.81 e Th/U = 3.81–4.58), with subordinate evidence of sedimentary recycling (Th/Sc = 0.77–1.35, Zr/Sc = 11.86–43.35) (Fig. 4E, F).

Two contrasting gneisses occur beneath the metasedimentary rocks. An epidote-bearing biotite gray gneiss with a homogeneous to slightly porphyroblastic texture, with apatite, titanite, and tonalitic composition. The other is a sillimanite-cordierite-bearing layered gneiss with alternating sillimanite-rich, cordierite, and biotite layers and granoblastic bands with quartz, plagioclase, and K-feldspar. The feldspars have idiomorphic shapes, suggesting a high-grade metamorphic origin.

The SiO_2 and $Na_2O + K_2O$ contents of the orthogneisses are variable (SiO_2 = 52.53–75.09 % and $Na_2O + K_2O$ = 4.22–8.02 %) leading to a variable classification of these rocks as granite/granonodiorite to syenodiorite, with some of the samples plotting outside the diagram (Fig. 6A). In classifications diagrams the samples are compatible with peraluminous orthogneiss (A/CNK = 0.98–2.07 and A/NK = 1.60–2.66) of the calc-alkaline series (A = 36.99–52.41; F = 34.23–44.86; M = 12.00–18.96) (Fig. 6B, C).

The samples present strong fractionation of REE (La_N/Yb_N = 9.03–50.58), with enrichment in LREE (La_N/Sm_N = 3.69–4.34) and depletion in HREE (Gd_N/Yb_N = 1.76–4.69) (Fig. 6D). Negative Eu anomalies are observed (Eu/Eu* = 0.37–0.71) with no associated Ce anomalies. Tectonic discrimination diagrams suggest that the gneisses protoliths were associated with a volcanic arc environment (Fig. 6E).

4.2. Zircon U-Pb and Hf-O systematics

4.2.1. Nova Xavantina Metavolcano-sedimentary Sequence

The detrital zircon crystals of the two analyzed metarenite samples (n = 141; samples FPN-03 and FPN-05) have three well marked distinct sets of ages: (i) an older Archean subordinate group (2.9–2.5 Ga); (ii) a predominant Paleoproterozoic group (2.1–1.6 Ga), (iii) and a younger Neoproterozoic group (980–685 Ma) (Fig. 7C). The maximum depositional age (MDA) was set at 725 ± 10 Ma. The $\delta^{18}O$ values for the Neoproterozoic zircon crystals are quite variable ($\delta^{18}O$ = 4.80–8.24 ‰ with one outlier of 10.97 ‰) (Fig. 7A), while the $\varepsilon Hf_{(t)}$ values are all negative from -24 to −8 (Fig. 7B). The Statherian-Orosirian zircon grains yielded similar $\delta^{18}O$ values of 4.32–8.88 ‰ with few outliers of 9.04 ‰ and 10.47 ‰, while the $\varepsilon Hf_{(t)}$ values are less negative from -11 to −2. The other metarenite sample present very negative $\varepsilon Hf_{(t)}$ values from -29 to –22 for the Neoproterozoic zircon grains and negative to slightly positive values from -20 to + 3 for the Statherian-Orosirian crystals.

The metacalcarenite (n = 89; sample FPN-11A) has similar age pattern as the metarenites, with a main age concentration in the Paleoproterozoic (2.1–1.7 Ga) with a main peak around 1.9 Ga (Fig. 7C). The Tonian to early Cryogenian ages are also important (950–690 Ma), with two main peaks at ca. 900 Ma to 740 Ma. The Mesoproterozoic ages are absent. The maximum depositional age for this sample was set at 735 ± 4 Ma. Tonian to early Cryogenian zircon grains present negative $\varepsilon Hf_{(t)}$ values from -12 to −4 (Fig. 7B) while the Tonian ones exhibit more negative $\varepsilon Hf_{(t)}$ values from –32 to −15. The Paleoproterozoic crystals also show negative $\varepsilon Hf_{(t)}$ from -24 to −4.

The detrital zircon grains of the lithic metarenites (n = 134; samples MNX-6 and MNX-11A) exhibit a distinct age pattern with the presence of Mesoproterozoic crystals, which are absent in the metarenite samples (Fig. 7C). Sample MNX-11A has a main group of ages varying from the Orosirian to the Ectasian (2010–1350 Ma), with a main age peak at approximately 1960 Ma. The predominant age group of sample MNX-6 varies from the Rhyacian to the Stenian (2125–1160 Ma), with a main

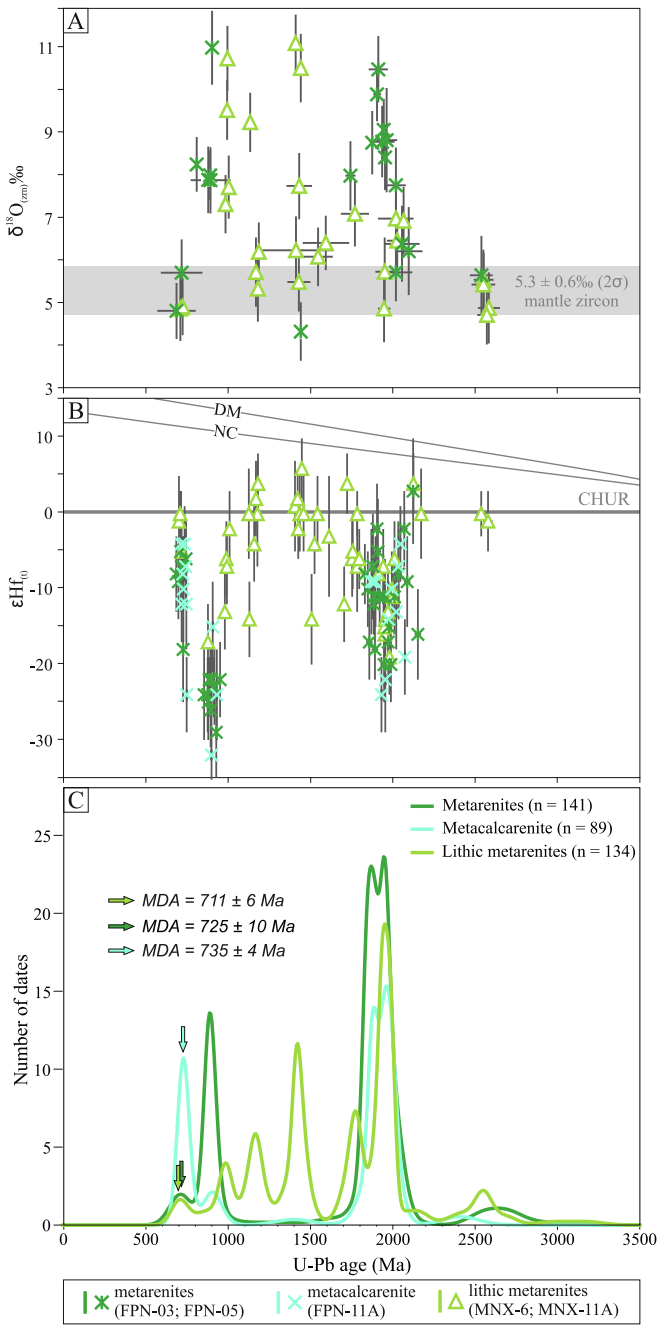

Fig. 7. Diagrams for the Nova Xavantina Metavolcano-sedimentary Sequence. (A) $\delta^{18}O$ versus age diagram; (B) $\varepsilon Hf_{(t)}$ versus age diagram, and (C) U-Pb histogram. MDA = maximum depositional age.

age peak around 1940 Ma. Archean to Siderian ages were also obtained (3190–2375 Ma). The MDA of the lithic metarenites was set at 711 ± 6 Ma.

Oxygen isotope and Lu-Hf analyses were conducted on one of the lithic metarenite samples (MNX-6), whereas the other was analyzed only for Lu-Hf (MNX-11A). The younger cluster zircon crystals yielded narrow low $\delta^{18}O$ values of 4.8–4.9 ‰ (Fig. 7A) and chondritic $\varepsilon Hf_{(t)}$ values of 0) (Fig. 7B), suggesting a less evolved origin of the sediment source. Tonian zircon grains and the youngest Stenian one yielded higher $\delta^{18}O$ values of 7.30–10.72 ‰ with $\varepsilon Hf_{(t)}$ values from -14 to −6, while the Stenian crystals yielded lower $\delta^{18}O$ values of 5.32–6.18 ‰ and $\varepsilon Hf_{(t)}$ values from 0 to + 4. Calymmian grains present two outliers with high $\delta^{18}O$ values of 10.5–11.1 ‰ and chondritic $\varepsilon Hf_{(t)}$ values of 0, while the main age peak present lower $\delta^{18}O$ values of 5.48–7.73 ‰ with $\varepsilon Hf_{(t)}$ values from -1 to + 1. Siderian to Orosirian zircon grains exhibit the lowest $\delta^{18}O$ values ($\delta^{18}O$ = 4.71–5.99 ‰) with $\varepsilon Hf_{(t)}$ values from -7 to 0. The Lu-Hf analyses of the other sample resulted in $\varepsilon Hf_{(t)}$ value of −17 for a Tonian crystal, −4 and + 2 for Stenian grains, −14 and 0 for Calymmian zircon crystals, and −19 and + 4 for the older grains.

4.2.2. *Bom Jardim de Goiás Metavolcano-sedimentary Sequence*

The orthogneiss sample (n = 27; sample FP-90A) has predominantly Neoproterozoic zircon crystals (955–585 Ma; n = 22; 2σ errors = 7–14 Ma), with a prevalence of ages of 698–611 Ma (n = 16) (Fig. 8A). Subordinate Archean-Mesoproterozoic ages vary from 2543 to 1012 Ma (n = 5; 2σ errors = 58–86 Ma) (Fig. 8A).

Most of the zircon crystals that yielded Cryogenian-Ediacaran ages (693–620 Ma) have $\varepsilon Hf_{(t)}$ values of -7 and 0 ($^{176}Hf/^{177}Hf_{(t)}$ = 0.28216–0.28237), with three outliers of 717, 661, and 658 Ma with $\varepsilon Hf_{(t)}$ values of + 3, –22, and + 7, respectively ($^{176}Hf/^{177}Hf_{(t)}$ = 0.28173– 0.28256) (Fig. 8A). The prevalent $\delta^{18}O$ values of this group vary from 6.5 ‰ to 9.5 ‰ (717–585 Ma), with one outlier of 10.3 ‰ (698 Ma) (Fig. 8A).

The main 698–611 Ma ages overlap within 2σ errors, spread along the Concordia (Fig. 8A detail). Spreading in the Concordia might reflect a protracted zircon crystallization process or a Pb loss episode after crystallization (Andersen et al., 2019). A well-defined $^{176}Hf/^{177}Hf_{(t)}$ signature between 0.28216 and 0.28237 suggests that zircon crystals with ages between 693 and 620 Ma comprise a single population affected by decoupling between U-Pb and Lu-Hf systems, supporting the Pb loss hypothesis (Andersen et al., 2019; Tedeschi et al., 2023). Therefore, the weighted average age of the group may not reflect the crystallization age of the protolith. Hence, we considered the oldest concordant U-Pb age of 698 ± 8 Ma as the minimum crystallization age of the Bom Jardim de Goiás orthogneiss (Fig. 8A detail), following the procedures described by Tedeschi et al. (2023). Zircon grains with older single ages between 2549 and 717 Ma were considered inherited crystals.

4.2.3. *Cuiabá Group*

Four metarenites and one schist from the Cuiabá Group were analyzed. The four metapsammitic rocks were classified into two groups based on their geographic location and age patterns.

The southern metarenites (n = 156; samples FPN-16 and FPN-32) have a late Paleoproterozoic to early Neoproterozoic interval of detrital ages (2100–895 Ma). Subordinate Archean ages (3.0–2.5 Ga) were also identified. The MDA was set at 900 ± 10 Ma.

The northwestern metarenites (n = 151; samples FPN-46 and FPN-54) have a main Mesoproterozoic source (1580–1000 Ma) with secondary, but not less important, Neoproterozoic (990–700 Ma) and Paleoproterozoic (2100–1600 Ma) sources (Fig. 9C). The MDA for this group of samples was set at 910 ± 7 Ma.

The chlorite-plagioclase-quartz-graphite-muscovite schist sample (n = 97; MNX-03) has a similar age distribution, with a main Mesoproterozoic age peak (ca. 1515 Ma) and less prominent ones (ca. 1010, 1165, and 1235 Ma) (Fig. 9C). Two older clusters of Paleoproterozoic data present ages of ca. 1760 Ma and 1905 Ma. The MDA for this sample was set at 948 ± 9 Ma.

Late Mesoproterozoic to Neoproterozoic zircon crystals yielded intermediate $\delta^{18}O$ values of 5.83–8.28 ‰ (Fig. 9A) and $\varepsilon Hf_{(t)}$ values from -3 to + 2 with an outlier of −21 (Fig. 9B). Calymmian grains yielded low to intermediate $\delta^{18}O$ values of 4.79–8.58 ‰ with $\varepsilon Hf_{(t)}$ values from -6 to −1. The older grains present higher $\delta^{18}O$ values of 4.59–10.27 ‰, and more negative $\varepsilon Hf_{(t)}$ values from -17 to −3. The Lu-Hf results from the other metarenite samples (Fig. 9B) exhibit more slightly negative $\varepsilon Hf_{(t)}$ values for the younger grains of late Mesoproterozoic to Neoproterozoic age ($\varepsilon Hf_{(t)}$ = -27 to + 4). The Calymmian ones also exhibit negative to slightly positive $\varepsilon Hf_{(t)}$ values from -15 to + 3 with an outlier with + 9. The older zircon crystals exhibit also negative $\varepsilon Hf_{(t)}$ values from -19 to 0.

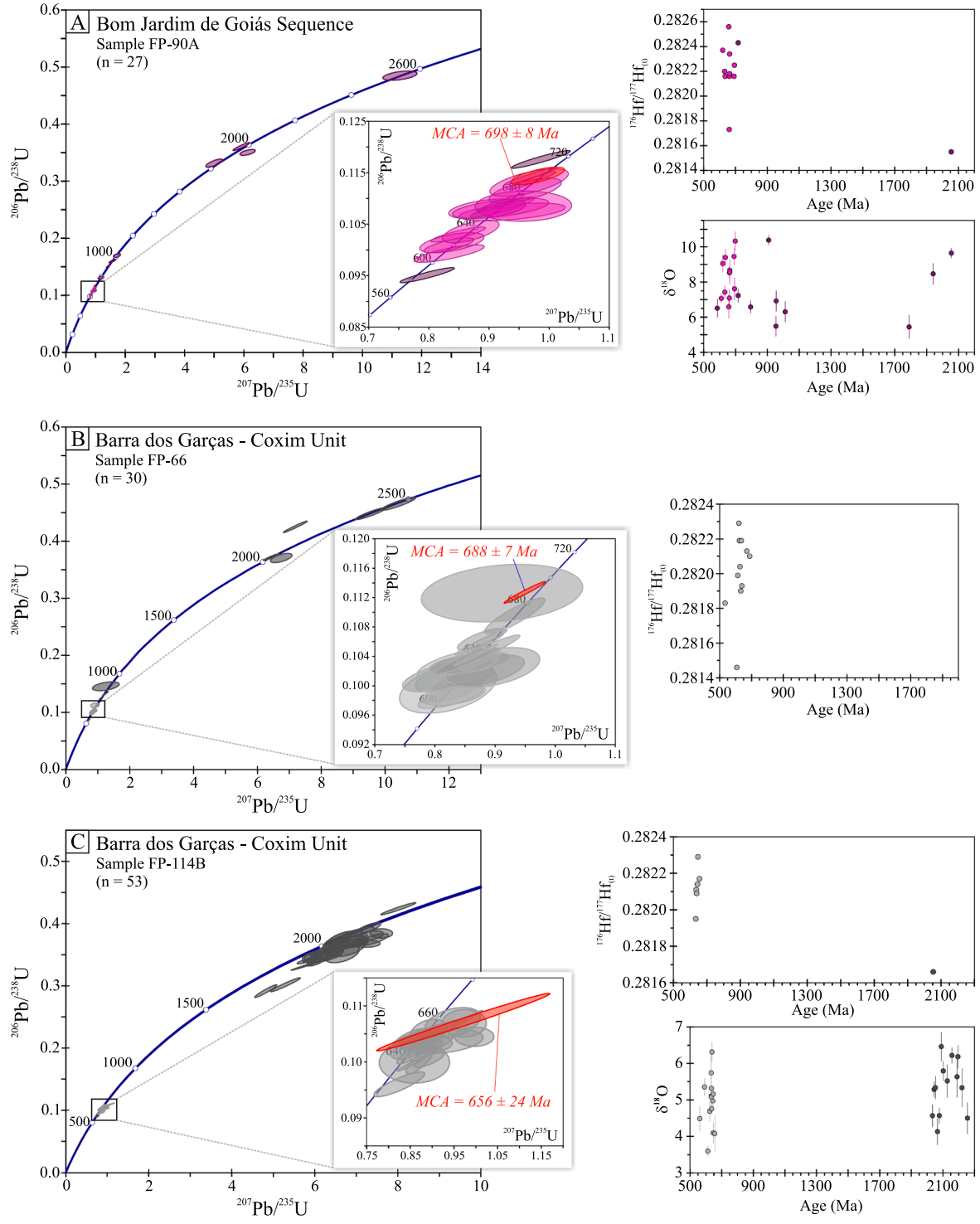

Fig. 8. Diagrams for the orthogneisses. (A) Tera-Wasserburg diagram of all orthogneisses of the Bom Jardim de Goiás Sequence with highlight of the 698 ± 8 Ma lower intercept; (C) Tera-Wasserburg diagram of all ms-bt-sill-plg-cdr-qtz-kfs gneiss data (Barra do Garças-Coxim Unit) with highlight of the 688 ± 7 Ma lower intercept; (E) Tera-Wasserburg diagram of all ttn-ep-ms-bt-plg-qtz gneiss data with highlight of the 656 ± 24 Ma lower intercept. MCA = minimum crystallization age.

The metapelite sample shows similar ranges of $\varepsilon Hf_{(t)}$ values (Fig. 9B) in which the younger grains exhibit very negative to slightly positive $\varepsilon Hf_{(t)}$ values from –23 to + 4, the Calymmian crystals tend to have less negative $\varepsilon Hf_{(t)}$ values from-5 to + 2, and the older ones present more negative $\varepsilon Hf_{(t)}$ values of -17 and −5.

4.2.4. *Barra do Garças-Coxim Unit*

U-Pb analyses of the four analyzed metapelites of this unit (n = 248; samples FPN-61, FP-79, FP-108B, and FP-111) point to very similar age patterns, with their main populations in the Neoproterozoic with important peaks in the Ediacaran (590–535 Ma and 675–600 Ma) and

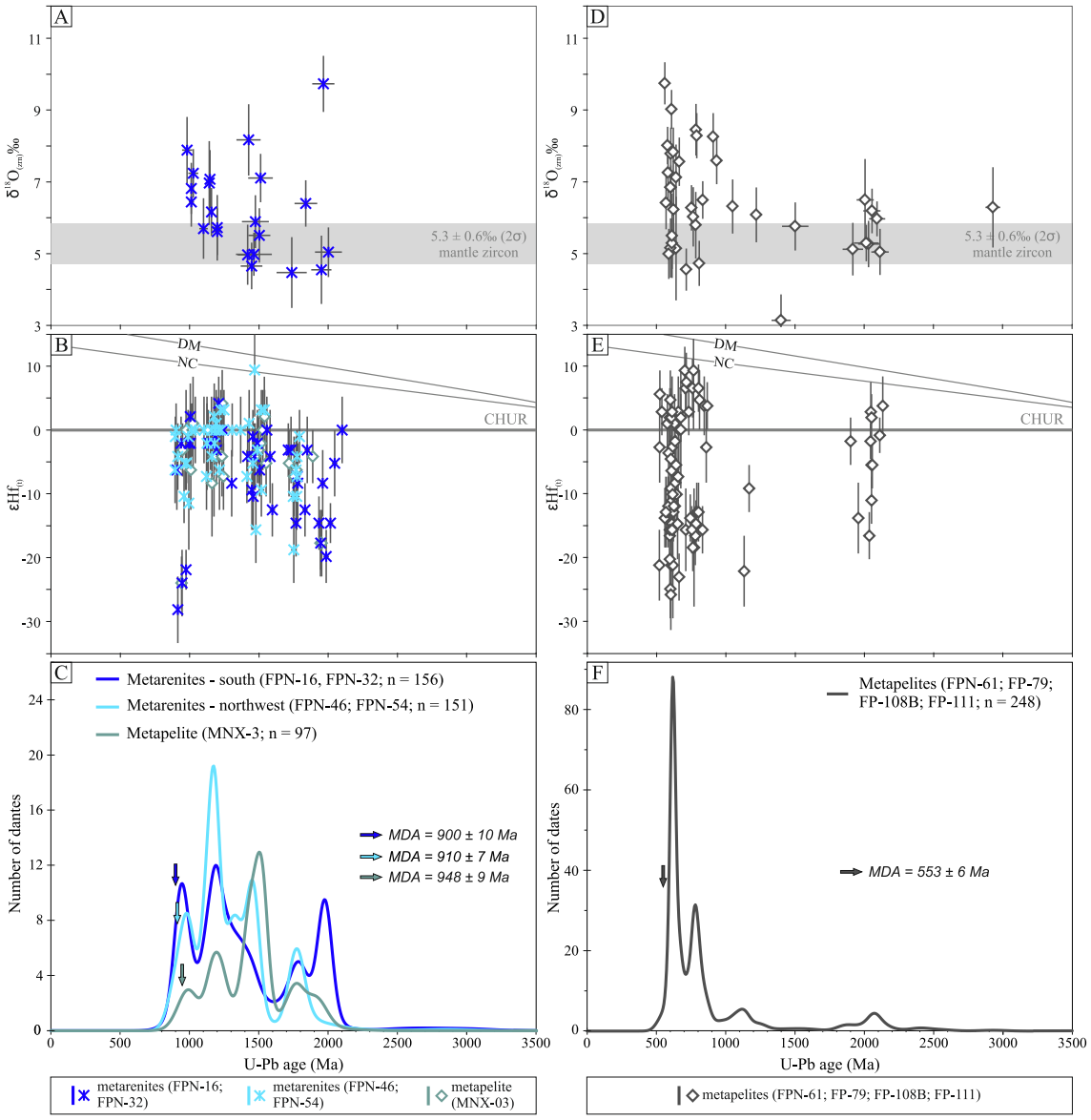

Fig. 9. Diagrams for the Cuiabá Group and Barra do Garças-Coxim Unit. (A) $\delta^{18}O$ versus age diagram; (B) $\varepsilon Hf_{(t)}$ versus age diagram; (C) U-Pb histogram of the Cuiabá Group; (D) $\delta^{18}O$ versus age diagram; (E) $\varepsilon Hf_{(t)}$ versus age diagram, and (F) U-Pb histogram of the Barra do Garças-Coxim Unit. MDA = maximum depositional age.

Cryogenian (800–765 Ma), and secondary peaks in the Tonian (970–865 Ma) (Fig. 9F). The MDA for the unit was set at 553 ± 6 Ma. The oxygen isotopes of the younger populations point to intermediate $\delta^{18}O$ values of 4.68–8.89 ‰ with only two outliers above 9.50 ‰ (Fig. 9D). The $\varepsilon Hf_{(t)}$ values of the same grains are very negative to positive ($\varepsilon Hf_{(t)}$ = -27 to + 7) (Fig. 9E). $\delta^{18}O$ values on the older zircon crystals are low to intermediate ($\delta^{18}O$ = 3.15–8.67 ‰) and $\varepsilon Hf_{(t)}$ values are negative from -18 to −2. The Lu-Hf data from the other metapelitic rock samples point to very negative to very positive $\varepsilon Hf_{(t)}$ values from -25 to + 10 for the younger ages and less negative and less positive $\varepsilon Hf_{(t)}$ values from -17 to + 5 for the older ages.

The zircon crystals of one of the analyzed orthogneisses (n = 30; sample FP-66) yielded Cryogenian–Ediacaran ages of 688–605 Ma (n = 21; 2σ errors = 6–18 Ma), which spread along the Concordia (Fig. 8B). Subordinate Paleoproterozoic (2479–1993 Ma; n = 5), Tonian (878–762 Ma; n = 3), and late Cambrian (534 Ma; n = 1) ages were also obtained (Fig. 8B). The $\varepsilon Hf_{(t)}$ values of the Cryogenian-Ediacaran group of ages (688–613 Ma) are negative ($\varepsilon Hf_{(t)}$ = -16 to −3; $^{176}Hf/^{177}Hf_{(t)}$ = 0.28119–0.28229) (Fig. 8B) with a very negative outlier ($\varepsilon Hf_{(607)}$ = –32; $^{176}Hf/^{177}Hf_{(607)}$ = 0.28146).

U-Pb ages on zircon crystals from the other orthogneiss (n = 53; sample FP-114B) define two main groups: (i) Rhyacian-Orosirian (2269–1953 Ma; n = 31; 2σ errors = 91–300 Ma) and (ii) Cryogenian-Ediacaran (656–561 Ma; n = 22; 2σ errors = 12–48 Ma) (Fig. 8C). The younger age group present negative $\varepsilon Hf_{(t)}$ values from -10 to −6 ($^{176}Hf/^{177}Hf_{(t)}$ = 0.28209–0.28217) (Fig. 8C) with three outliers ($^{176}Hf/^{177}Hf_{(t)}/\varepsilon Hf_{(t)}$ = 0.28195/-15 for t = 633 Ma; 0.28229/-2 for t = 646 Ma; and 0.28249/+3 for t = 629 Ma). One 2052 Ma-aged crystal has a positive $\varepsilon Hf_{(t)}$ value of +6 ($^{176}Hf/^{177}Hf_{(t)}$ = 0.28166). The $\delta^{18}O$ values of the Neoproterozoic group (655–561 Ma) are very low ($\delta^{18}O$ = 3.6–6.3 ‰), while $\delta^{18}O$ values of the Paleoproterozoic range (2256–2034 Ma) are slightly higher ($\delta^{18}O$ = 4.1–6.5 ‰) (Fig. 8C).

Both orthogneiss samples have Cryogenian-Ediacaran sets of ages with evidence of Pb loss and U-Pb/Lu-Hf decoupling, that is, a well-defined $^{176}Hf/^{177}Hf_{(t)}$ signature for a wide U-Pb date interval. The oldest concordant date defines minimum crystallization ages of 688 ± 7 Ma for sample FP-66 (Fig. 8B detail) and of 656 ± 24 Ma for sample FP-114B (Fig. 8C detail). The younger late Cambrian date of sample FP-66 was obtained from the rim of the crystal and is probably related to the 545–535 Ma metamorphic event that affected the area (Geraldes et al.,

2008). Dates older than the Cryogenian-Ediacaran group are considered inherited because they are commonly found in the schists of the unit (Fig. 9F).

4.3. Whole-rock Nd-Sr data

The NdT_{DM} model ages of the metasedimentary rocks of the Nova Xavantina Metavolcano-sedimentary Sequence are Rhyacian to Calymmian (2.18–1.55 Ga), with associated negative $\varepsilon Nd_{(710)}$ values from -12.4 to −7.6 (t = 710 Ma = MDA; see item 4.2.1) (Fig. 10A) and $^{87}Sr/^{86}Sr$ values from 0.7122 to 0.7437. The two-stage NdT_{DM} model ages of the metavolcanic rocks of the same unit are Rhyacian (2.27–2.13 Ga), with negative $\varepsilon Nd_{(750)}$ values from -12.5 to −10.1 (t = 750 Ma determined by Silva, 2018) and $^{87}Sr/^{86}Sr$ values between 0.7060 and 0.7272. The lithic metarenites also present Rhyacian NdT_{DM} model ages (2.22–2.14 Ga), with negative $\varepsilon Nd_{(710)}$ values from -11.9 to −10.6 and $^{87}Sr/^{86}Sr$ values of 0.7142 and 0.7191.

The two-stage NdT_{DM} model ages of the six metavolcanic rocks of the Bom Jardim de Goiás Metavolcano-sedimentary Sequence might be separated into two groups. The older group, with Statherian NdT_{DM} model ages of 1.76–1.61 Ga, has negative $\varepsilon Nd_{(750)}$ values from -4.7 to −2.6 (t = 750 Ma is the MDA determined by Guimarães et al., 2012) and $^{87}Sr/^{86}Sr$ values between 0.7037 and 0.7093. The younger group, with Stenian NdT_{DM} model ages of 1.16–1.03 Ga, has positive $\varepsilon Nd_{(750)}$ values from +2.8 to + 4.3 (Fig. 10B) and $^{87}Sr/^{86}Sr$ values between 0.7053 and 0.7061. The three metatuff samples present Stenian-Tonian NdT_{DM} model ages (1.12–0.91 Ga), with associated positive $\varepsilon Nd_{(750)}$ values from +3.26 to + 5.60 and $^{87}Sr/^{86}Sr$ values between 0.7072 and 0.7188. The gneiss from the same unit has the oldest NdT_{DM} model age (2.15 Ga), with a negative $\varepsilon Nd_{(700)}$ value of -5.45 (t = 700 Ma which is the

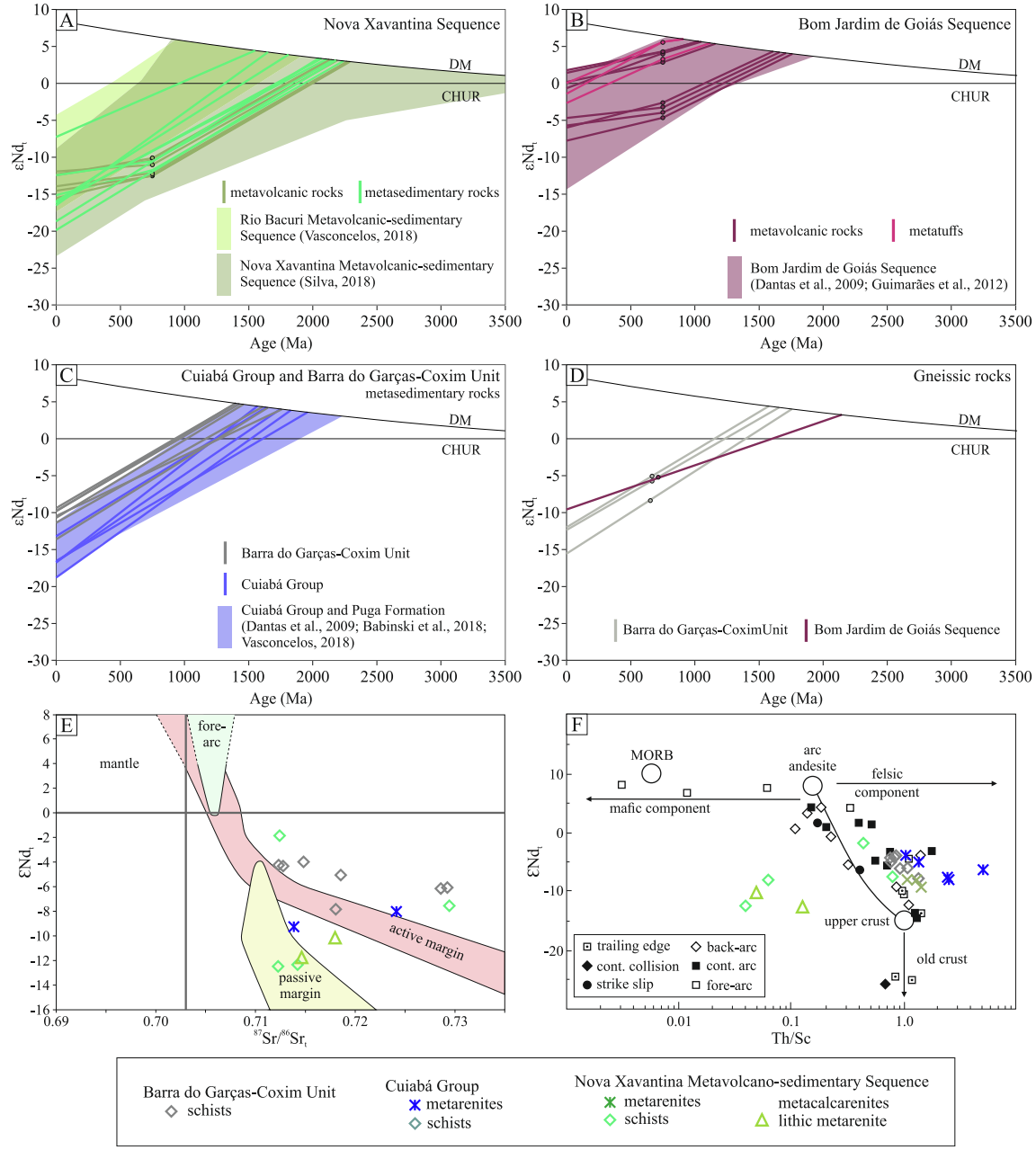

Fig. 10. $\varepsilon Nd_{(t)}$ versus age of the diagrams: (A) Nova Xavantina Metavolcano-sedimentary Sequence; (B) Bom Jardim de Goiás Metavolcano-sedimentary Sequence; (C) Cuiabá Group and Barra do Garças-Coxim Unit; and (D) gneissic rocks; (E) $\varepsilon Nd_{(t)}$ versus $^{87}Sr/^{87}Sr_{(t)}$ and (F) $\varepsilon Nd_{(t)}$ versus Th/Sc diagrams for the studied metasedimentary rocks.

crystallization age; see item 4.2.2) and a $^{87}Sr/^{86}Sr$ value of 0.7050.

The NdT_{DM} model ages of the metarenites and schists of the Cuiabá Group are Orosirian-Statherian (1.83–1.64 Ga), with associated negative $\varepsilon Nd_{(900)}$ values from -7.3 to −3.6 (t = 900 Ma = MDA; see item 4.2.3) and $^{87}Sr/^{86}Sr$ values between 0.7389 and 0.7792 (Fig. 10C).

The NdT_{DM} model ages of the metasedimentary rocks of the Barra do Garças-Coxim Unit present a narrow interval in the Statherian-Calymmian (1.76–1.40 Ga), with negative $\varepsilon Nd_{(553)}$ values from -7.6 to −3.8; t = 553 Ma = MDA; see item 4.2.4) (Fig. 10C) and $^{87}Sr/^{86}Sr$ values between 0.7122 and 0.7292. The NdT_{DM} model ages of the gneiss samples are also Statherian-Calymmian (1.76–1.58 Ga), with slightly more negative $\varepsilon Nd_{(t)}$ values ($\varepsilon Nd_{(690)}$ = -7.96 and $\varepsilon Nd_{(655)}$ = -5.87; see item 4.2.4) and $^{87}Sr/^{86}Sr$ values between 0.7154 and 0.7301.

5. Discussion

Field relations, elemental and isotopic geochemistry, and geochronological data support the division of the Eastern Paraguay Belt domain into four tectonostratigraphic units: (i) the Nova Xavantina Metavolcano-sedimentary Sequence, (ii) the Cuiabá Group, (iii) the Barra do Garças-Coxim Unit, and (iv) the Bom Jardim de Goiás Metavolcano-sedimentary Sequence. The latter unit is located east of the Transbrasiliano Lineament, forming part of the Brasília Orogen (Fig. 2). This study suggests that the area of occurrence of the Nova Xavantina Metavolcano-sedimentary Sequence is more restricted than previously believed (Silva, 2007, 2018). Most of the rocks in the area belong to the Cuiabá Group, as proposed by Sousa et al. (2019).

The rocks of the Barra do Garças-Coxim Unit have been reported in the literature as an undivided sub-unit of the Cuiabá Group (Campanha et al., 2011; Babinski et al., 2018). The present study and previous results (Pelosi, 2017; McGee et al., 2018; Vasconcelos, 2018) indicate that this unit is geochemically and geochronologically distinct from the Cuiabá Group. This suggests a source area for the collisional uplift of the Brasília Orogen (800–600 Ma) located at the Paranapanema Block edge as well as in the Cambrian plutonic rocks of the inner Paraguay Belt (Godoy et al., 2010). Additionally, the Nd isotopic signature of samples from the Cuiabá Group is similar to that reported for the Puga Formation (Dantas et al., 2009; Babinski et al., 2018; Vasconcelos, 2018). However, the Nd isotopic signature of samples from the Barra do Garças-Coxim Unit has younger NdT_{DM} model ages and less negative εNd_0, although

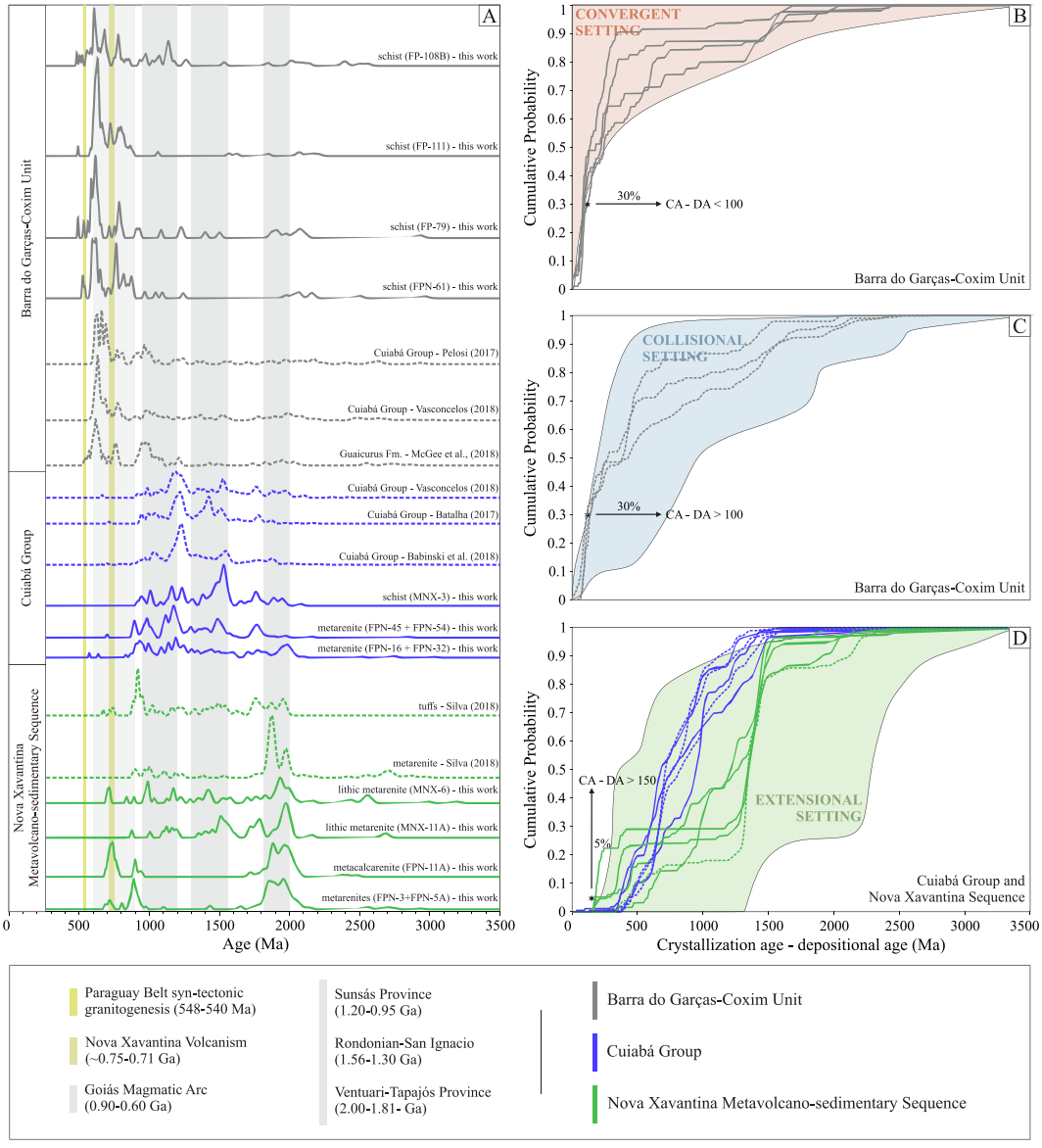

Fig. 11. (A) Histograms of all analyzed samples together with data from bibliography. Cumulative probability plots for (B) convergent; (C) collisional, and (D) extensional settings (Cawood et al., 2012).

the $\varepsilon Nd_{(t)}$ are similar.

5.1. Provenance and maximum depositional age

The rocks from the Nova Xavantina Metavolcano-sedimentary Sequence predominantly have ages between 2.1–1.8 Ga, with additional sources with 1.50–1.35 Ga and 1.0–0.7 Ga. These results, along with available previous data (Silva, 2018), suggest that the lithic metarenites represent the erosion of a late Paleoproterozoic to Mesoproterozoic basement, with contributions from Tonian-Cryogenian volcanic detritus (Fig. 11A). Similarly, metarenites and metacalcarenites of the same unit indicate the erosion of an Orosirian basement with significant influence of Tonian rocks. The oldest ages can be found in the Amazonian Craton, suggesting erosion from the Tapajós and Juruena orogens, the Uatumã and Alta Floresta silicic large igneous provinces (SLIPs), the Santa Helena/Alto Guaporé arcs and, to a lesser extent, from the Rondonian tin province (Johansson et al., 2022 and references therein). Negative $\varepsilon Nd_{(t)}$ values and variant Th/Sc ratios suggest both mafic igneous depleted mantle and quartzose upper crust provenances. The Neoproterozoic detritus likely originated in the Paranapanema Block, where the Goiás Magmatic Arc was a nearby active volcanic arc during the depositional period, and from the volcanic rocks of the Nova Xavantina Sequence itself. The younger age of the lithic metarenites (ca. 710 Ma) marks the lower boundary of the Nova Xavantina magmatism that started around 750 Ma (Silva, 2018). The geochemical signature of these rocks indicates an E-MORB affinity and shallow magmatic sources (Fig. 5), whereas the whole-rock Nd-Sr data place them between passive and active margin arrays. This young age is also observed within the errors of the metarenites.

The metavolcanic rocks and metatuffs of the Bom Jardim de Goiás Sequence have volcanic arc affinities with magma-crust interaction and deep magmatic sources (Fig. 5). Guimarães et al. (2012) reported Nd data with juvenile signature. The orthogneiss sample has ca. 700 Ma and is chemically related to a volcanic arc.

Although they have similar magmatic ages of ca. 750 Ma (Guimarães et al., 2012; Silva, 2018; this work), the metavolcanic rocks from both sequences exhibit different geochemical characteristics, suggesting distinct tectonic environments. The Nova Xavantina Sequence may be related to an opening rift, whereas the Bom Jardim de Goiás rocks may be associated with a magmatic arc.

The analyses of metarenites and a schist from the Cuiabá Group reveal that the main sources are of Paleoproterozoic to early Tonian ages, with age clusters of 1.2–0.9 Ga, 1.55–1.45 Ga, 1.80–1.75 Ga, and 2.0–1.9 Ga. These age patterns are related to the Sunsás Province, the Santa Helena/Alto Guaporé arcs, the Juruena and Tapajós orogens, and the Alta Floresta/Uatumã SLIPs (Fig. 11A). Similar age patterns have been observed in the Northern Paraguay Belt (McGee et al., 2015b; Babinski et al., 2018; Batalha, 2017; Vasconcelos, 2018; Johansson et al., 2022), with prominent peaks at 1.3–1.2 Ga. Tonian detrital zircon grains with ages of 0.9–0.8 Ga may indicate an influence of the Goiás Magmatic Arc although as a more distal source. This younger age cluster is less pronounced in the Cuiabá Group than in the Nova Xavantina Sequence.

The analyzed metasedimentary samples of the Barra do Garças-Coxim Unit show a significant presence of Neoproterozoic sources (Dorilêo-Leite et al., 2024; this work), with ages around 0.65–0.60 Ga and 0.85–0.75 Ga. These Tonian-Cryogenian ages (Fig. 11A) were primarily derived from the Goiás Magmatic Arc, which continued to contribute to sediments until ca. 610 Ma, and from the metamorphic and magmatic rocks of the Brasília Orogen. Younger Cambrian-Ediacaran ages are believed to have been originated from *syn*-orogenic granitic plutons within the inner domains of the Paraguay Belt. There is also a secondary influence from Paleoproterozoic sources with ages of 2.10–2.05 Ga, also reported in the Arenópolis Magmatic Arc (Carneiro et al., 2021). These immature rocks are chemically and isotopically compatible with sediments derived from active margin environments (Fig. 4C and 10E).

The 690–655 Ma high-grade metamorphic cordierite-sillimanite-bearing gneiss and epidote-bearing metatonalite are considered to be basement rocks and part of the Goiás Magmatic Arc. They have chemical affinities with within-plate anomalous ocean ridges and volcanic arcs (Fig. 6E).

Our new results for the Eastern Paraguay Belt indicate maximum depositional ages of 711 ± 6 Ma, 900 ± 10 Ma and 553 ± 6 Ma for the Nova Xavantina Metavolcano-sedimentary Sequence, the Cuiabá Group and the Barra do Garças-Coxim Unit, respectively. The maximum depositional age obtained for the Cuiabá Group, and the Puga Formation are between 700 and 640 Ma (Babinski et al., 2013, 2018; McGee et al., 2015b, 2018). The Barra do Garça-Coxim Unit is correlated with the inner and allochthonous units of the Cuiabá Group (Campanha et al., 2011) that displays a young maximum depositional age of 600–540 Ma (Pelosi, 2017; McGee et al., 2018; Vasconcelos, 2018).

5.2. Hf-O isotope data

By comparing the zircon Hf and oxygen results (Fig. 12), it is possible to highlight distinct patterns for the four units. The lithic metarenite from the Nova Xavantina Sequence suggests a mantle-derived source for its young zircon grains with ca. 710 Ma (Fig. 12A) and input of supracrustal older material observed through the negative correlation between $\delta^{18}O$ and $\varepsilon Hf_{(t)}$. The metarenite sample does not provide any correlation between the two isotopic reservoirs; it suggests an important supracrustal source with lower values of $\varepsilon Hf_{(t)}$ and higher values of $\delta^{18}O$.

The orthogneiss sample from the Bom Jardim de Goiás Sequence presents $\varepsilon Hf_{(t)}$ values between −10 and + 7 and $\delta^{18}O$ values of 6-10 ‰ (Fig. 12B), suggesting magmatic differentiation or input of supracrustal material.

The Cuiabá Group metarenite sample suggests a depleted mantle-like source for its Mesoproterozoic zircon grains and a more radiogenic material for the other crystals (Fig. 12C). The metapelites of the Barra do Garças-Coxim Unit presented a negative correlation, suggesting an evolution trend from a depleted mantle-derived source to a more evolved supracrustal-like source (Fig. 12D), with a highlight for two zircon grains with ca. 710 Ma and 810 Ma with a mantle signature. The gneisses of the basement have low $\delta^{18}O$ values and variable $\varepsilon Hf_{(t)}$ between −15 and + 6. The observed trend suggests magmatic differentiation through mantle-derived sources and the important preservation of juvenile isotopic signatures (Fig. 12D).

5.3. Tectonic evolution

An extensional regime (Fig. 11D) is suggested for the Nova Xavantina Sequence development, while its volcanic activity occurred concurrently with the subduction-related volcanic arc in the far eastern Bom Jardim de Goiás Sequence. Interestingly, the siliciclastic and carbonatic rocks revealed different sedimentary provenances: the Amazonian Craton in the west and the Goiás Magmatic Arc in the east, respectively. These tectonic relationships suggest a back-arc setting at 750–700 Ma, with a marginal basin spreading, separating the Amazonian and Paranapanema paleoplates (Fig. 13A). This highlights the role of the closing processes of the Goiás-Pharusian Ocean in the local Rodinia break-up, untangling competing scenarios of crust addition and accretionary orogeny. The evolution of the marginal basin was likely related to the coeval ophiolite sequence of the ocean-passive margin transition in the Araguaia Belt (Hodel et al., 2019). It may also have promoted oceanic connections with the back-arc oceanic basin in the Pampean Orogen (Escayola et al., 2007).

The ocean between Laurentia and Gondwana is referred to as the Clymene Ocean (Trindade et al., 2006; Tohver et al., 2010), however, an alternative model proposes that the final assemblage of Gondwana occurred during the Ediacaran through the diachronic closure of the long-lasting Goiás-Pharusian Ocean (Cordani et al., 2013a). The present

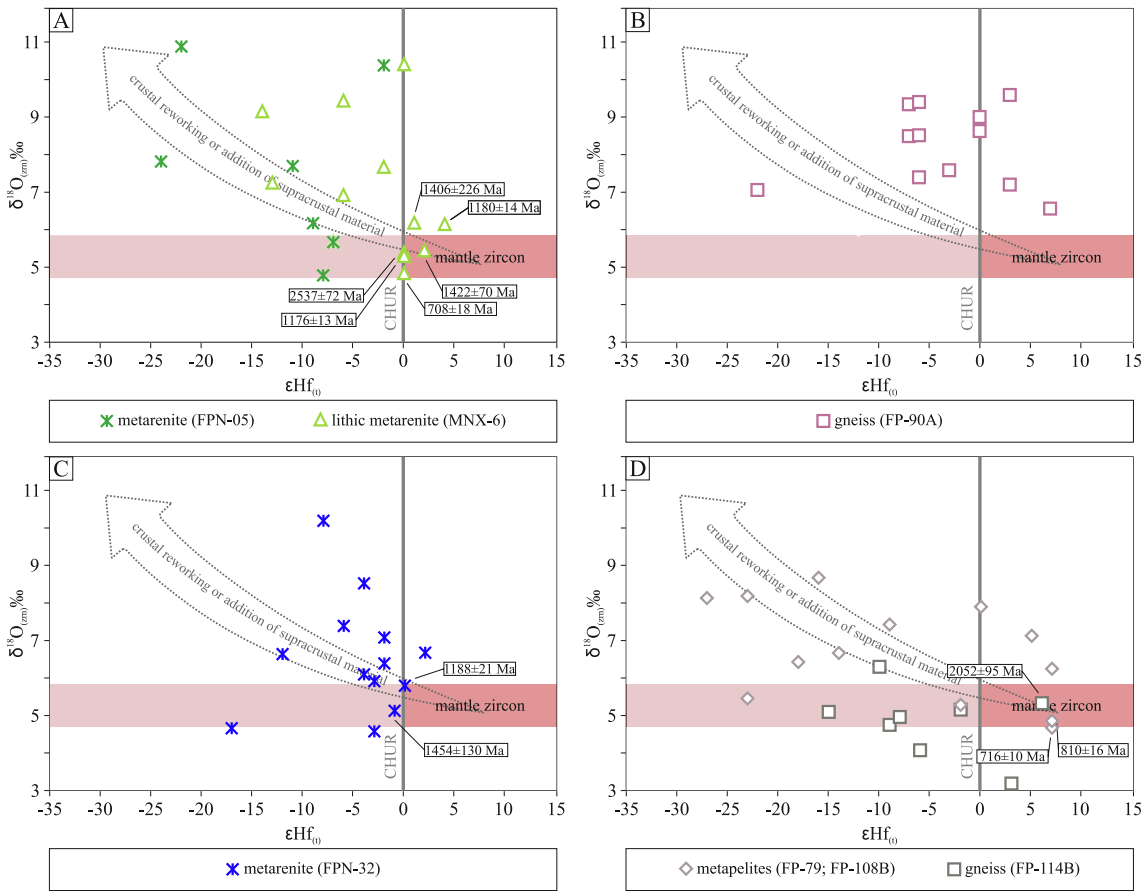

Fig. 12. $\delta^{18}O$ versus $\varepsilon Hf_{(t)}$ diagrams for the (A) Nova Xavantina Metavolcano-sedimentary Sequence; (B) the Bom Jardim de Goiás Metavolcano-sedimentary Sequence; (C) the Cuiabá Group, and (D) the Barra do Garças-Coxim Unit.

study proposes a connection between the history of the Clymene Ocean and the reorganization of plate movements during the closure of the Goiá-Pharusian Ocean.

The metasedimentary rocks of the Cuiabá Group were deposited under extensional tectonic regimes (Fig. 11D) through erosion, primarily from the Amazonian Craton, with a smaller contribution from the Brasília Orogen. Previous studies have reached the consensus that a passive margin environment (Fig. 13B) with oxic oceanic water circulation followed the extensive glaciation (Alvarenga et al., 2004; Boggiani et al., 2010; Viehmann et al., 2016; Frei et al., 2017; Freitas et al., 2021). The sedimentary record of this passive margin spans from the middle Cryogenian (after 690 Ma) to the end of the Ediacaran (542 Ma), registering all Neoproterozoic glacial epochs supported by U-Pb zircon ages (Babinski et al, 2018, and references therein) (Fig. 13C).

In the eastern Paraguay Belt, the extensional regime persisted until 580 Ma with alkaline metaultramafic intrusions (Silva, 2018). The transition to a contractional regime with eastward oceanic subduction and growth of the magmatic arc is marked by 555–535 Ma calc-alkaline granites (Godoy et al., 2010) (Fig. 12B, C, and 13D). The eastern margin of the Paranapanema Block acted as an active margin for the Paraguay Orogen (Fig. 13D, E). The 690–655 Ma high-grade gneisses of the basement of the foreland deposits support the continuity of the Goiás Magmatic Arc and the metamorphic rocks of the Brasília Orogen west of the Transbrasiliano Lineament.

The immature deposits of the Barra do Garça-Coxim Unit fill an intra-arc fore-deep trough. They were fed by the erosion of igneous and metamorphic rocks of the Goiás Magmatic Arc after 540 Ma, belatedly raised (Pelosi, 2017; Vasconcelos, 2018; McGee et al., 2018; Dorilêo-Leite et al., 2024; this work) and collisional sutures between the Amazonian and Paranapanema paleocontinents after 540 Ma (Fig. 13E), constrained by $^{40}Ar/^{39}Ar$ plateau ages on illite and micas (Geraldes et al., 2008; Tohver et al., 2012; Piacentini et al., 2013). Low-grade metamorphic foliation indicates basin inversion and emphasizes its fast deposition. The westward progression of the inner uplift in the Paraguay Orogen drives the foreland migration and subsequent back-bulge basin filling at the SE Amazonian Craton margin (Fig. 13A–E) (Bandeira et al., 2012; McGee et al., 2018).

The Cambrian closure of the Clymene Ocean between Laurentia and the previously assembled Río de la Plata, Paranapanema, and São Francisco cratons promoted the final suture zone of Western Gondwana.

It is reasonable to assume that this short-lived continental margin records the separation between the Paranapanema-Amazonian continental blocks, as a northern-northeastern continuity of the Puncoviscan Ocean. The marine-dominated sequences are covered by three distinct units: (i) the southern fossiliferous cratonic margin deposit, containing volcanic ashes of 555 Ma to 542 Ma (Parry et al., 2017); (ii) the northern

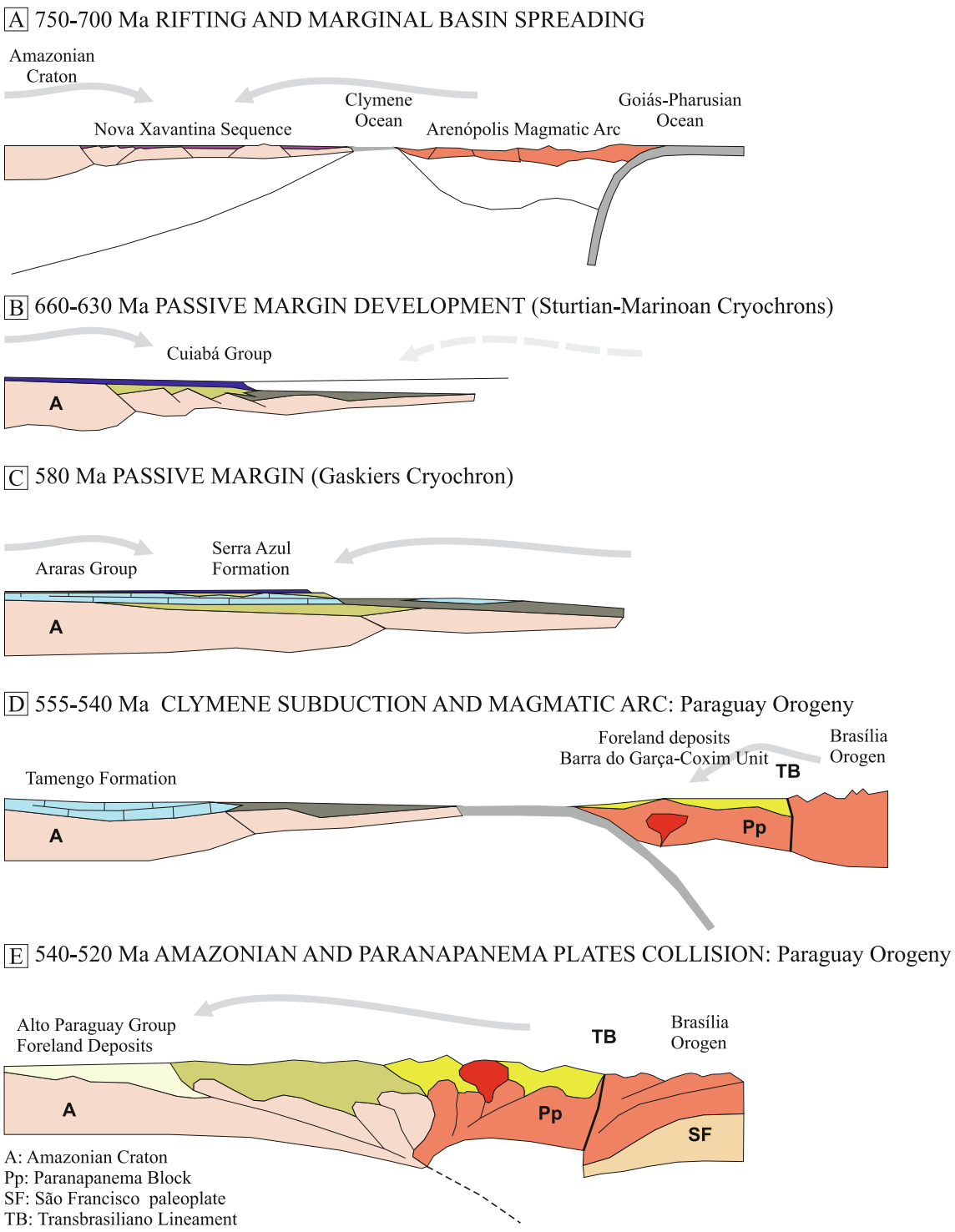

Fig. 13. Sketches of tectonic evolution: (A) Extensional regime marked by the ca. 750 Ma rifting of the Nova Xavantina Sequence, breaking apart the Amazonian and Paranapanema paleoplates; (B) Development of the passive margin domain and deposition of the Cuiabá Group during the Sturtian-Marinoan cryochrons; (C) Evolution of the passive margin during the Gaskiers cryochron; (D) Inversion to contractional regime and development of foreland deposits related to the subduction process; (E) Deposition of collision-controlled foreland deposits on the cratonic domain during collisional processes.

external deposits, which record a foreland basin also developed during the Ediacaran-Cambrian transition (Bandeira et al., 2012); (iii) and an internal sedimentary unit deposited between 580–540 Ma and metamorphosed under low-grade conditions (Pelosi, 2017; McGee et al., 2018; Dorilêo-Leite, et al., 2024; this work).

6. Conclusions

– The Nova Xavantina Metavolcano-sedimentary Sequence records a rift opening through bimodal volcanism depicted by juvenile Hf-O signatures on ca. 710 Ma zircon grains recorded by lithic metarenites and old evolved material on the whole-rock Nd signature of metavolcanic rocks. The results also suggest a mafic to upper crust origin with E-

MORB affinities emerging from shallow depths. Geochemical and geological data suggest an increase in the asthenosphere under the Amazonian-Paranapanema crustal lithosphere during the late Tonian in response to the subduction setting established at the easternmost edge of the Paranapanema paleoplate during the development of the Goiás Magmatic Arc. The 750–710 Ma rift volcanism and sedimentation may have lasted until at least 690 Ma, and the detritus recorded in the metasedimentary rocks was probably derived from the main Amazonian Craton provinces and the Goiás Magmatic Arc.

– The Bom Jardim de Goiás metavolcano–sedimentary sequence represents a juvenile arc accreted to the Goiás Magmatic Arc. The Hf-O-Nd signatures of the 685 Ma orthogneiss suggest evolution from depleted material.

– Based on geochemical records, rocks of the Cuiabá Group were deposited on the Amazonian cratonic passive margin and registered provenance from upper crust erosion with high rates of sedimentary recycling. The U-Pb record suggests the erosion of Mesoproterozoic rocks from the Sunsás Orogen, the Alto Guaporé and Santa Helena magmatic arcs, and Paleoproterozoic rocks from the Juruena and Tapajós orogens. However, the Neoproterozoic rocks of the Goiás Magmatic Arc also left records in zircon detrital grains. Nd-Hf-O isotopic signatures indicate the influence of less-evolved Mesoproterozoic sources, pointing to a juvenile-like area in the Amazonian Craton.

– The Barra do Garças-Coxim Unit, now separated from the Cuiabá Group, reflects the direct erosion of the Goiás Magmatic Arc, and marks the shift from an extensional to a contractional regime with a maximum depositional age of ca. 535 Ma. Geochemical data indicate similarities between the studied sediments and those found in volcanic arc settings through the erosion of felsic rocks with upper crust features. They were deposited over the Paranapanema Block and recorded the direct input of Cryogenian-Tonian juvenile material from Bom Jardim de Goiás Arc volcanism. The presence of Orosirian-Rhyacian material indicates erosion of the Goiás Massif or arc basement. The detritus originated from the 685 Ma orthogneiss in Bom Jardim de Goiás and the 630–615 Ma gneiss beneath the metasedimentary rocks of the unit suggest the extension of the Goiás Magmatic Arc to the west, beyond the Transbrasiliano Lineament.

– Detrital zircon age comparisons show that the lower and older units (Nova Xavantina and Bom Jardim de Goiás sequences) have predominantly Paleoproterozoic ages, around 2.1–1.9 Ga, with little or no Mesoproterozoic ages. Tonian ages are was also significant in these units. In contrast, the Cuiabá Group contains zircon grains with Mesoproterozoic ages, with limited data from the Tonian and late Paleoproterozoic. The Barra do Garças-Coxim Unit stands out for its Ediacaran-Cryogenian to late Tonian ages, further distinguishing it from the Cuiabá Group.

– The inversion regime from extensional to contractional during the Paraguay Belt formation, from the precursor basin to the deformed belt, would have occurred after ca. 550 Ma with the deposition of the Barra do Garças-Coxim unit and related magmatism.

CRediT authorship contribution statement

Gabriella Labate Frugis: Writing – original draft, Investigation, Formal analysis, Conceptualization. **Mario da Costa Campos Neto:** Writing – review & editing, Validation, Supervision, Resources, Funding acquisition, Conceptualization. **Alice Westin:** Writing – review & editing, Validation, Software, Data curation. **Christopher Mark Fanning:** Formal analysis.

Declaration of competing interest

The authors declare that they have no known competing financial interests or personal relationships that could have appeared to influence the work reported in this paper.

Data availability

I have shared all data as Supplementary Material

Acknowledgements

This research was supported by the *Fundação de Amparo à Pesquisa do Estado de São Paulo* – FAPESP (grants 2015/03737-0 and 2017/18174-6). M.C. Campos Neto is a fellow of the Brazilian Research Council (CNPq).

Appendix A. Supplementary material

Supplementary data to this article can be found online at https://doi.org/10.1016/j.precamres.2024.107529.

References

Almeida F.F.M. 1945. Geologia do Sudoeste Mato-Grossense. Rio de Janeiro, DNPM/DGM. 118 p. (Boletim 116).

Almeida F.F.M. 1964. Geologia do Centro-Oeste Matogrossense. Rio de Janeiro, DNPM7DGM. 137 p. (Boletim 215).

Almeida F.F.M. 1984. Província Tocantins -setor sudoeste. In: Almeida F.F.M. & Hasui Y. (eds.) O Pré-Cambriano do Brasil. São Paulo, Ed. Edgard Blucher, p. 265-281.

Alvarenga, C.J.S., 1988. Turbiditos e a glaciação do final do Proterozoico Superior no Cinturão Paraguai. Mato Grosso. Revista Brasileira De Geociências 18 (3), 323–327.

Alvarenga, C.J.S., Trompette, R. 1988. Upper Proterozoic glacial environment of the border of Amazonian Craton and its evolution towards the adjacent Paraguay Belt. (Mato Grosso, Brazil). In: Meeting Earth's Glacial Record-Proj. 260. Cuiabá, 1988. Abstracts and Field Trip. Cuiabá, IGCP-UNESCO/UFMT. p. 31-44.

Alvarenga, C.J.S., Saes, G., 1992. Estratigrafia e sedimentologia do Proterozóico Médio e Superior da região sudeste do Cráton Amazônico. Revista Brasileira De Geociências 22 (4), 493–499.

Alvarenga, C.J.S., Santos, R.V., Dantas, E.L., 2004. C-O-Sr isotopic stratigraphy of cap carbonates overlying Marinoan-age glacial diamictites in the Paraguay Belt, Brazil. Precambrian Research 131, 1–21.

Alvarenga, C.J.S., Trompette, R., 1992. Glacially influenced sedimentation in the Later Proterozoic of the Paraguay belt (Mato Grosso, Brazil). Paleogeography, Paleoclimatology, Paleoecology 92, 85–105.

Alvarenga, C.J.S., Trompette, R., 1993. Evolução tectônica brasiliana da Faixa Paraguai: a Estruturação da região de Cuiabá. Revista Brasileira De Geociências 23 (1), 18–30.

Alvarenga, C.J.S., Figueiredo, M.F., Babinski, M., Pinho, F.E.C., 2007. Glacial diamictites of Serra Azul formation (Ediacara, Paraguay belt): Evidence of the Gaskiers glacial event in Brazil. Journal Od South American Earth Sciences 23, 236–241.

Andersen, T., Elburg, M.A., Magwaza, B.N., 2019. Sources of bias in detrital zircon geochronology: Discordance, concealed lead loss and common lead correction. Earth-Science Review 197, 102899. https://doi.org/10.1016/j.earscirev.2019.102899.

Angerer, T., Hagemann, S.G., Walde, D.H.G., Halverson, G.P., Boyce, A.J., 2016. Multiple metal sources in the glaciomarine facies of the Neoproterozoic Jacadigo iron formation in the "Santa Cruz deposit", Corumbá, Brazil. Precambrian Research 275, 369–393.

Azevedo, P.R., Rocha, M.P., Soares, J.E.P., Fuck, R.A., 2015. Thin lithosphere between the Amazonian and São Francisco cratons, in central Brazil, revealed by seismic P-wave tomography. Geophysical Journal International 201, 61–69.

Babinski, M., Boggiani, P.C., Fanning, C.M., Fairchild, T.R., 2008. U-Pb SHRIMP geochronology and isotope chemostratigraphy (C, O, Sr) of the Tamengo Formation, southern Paraguay belt, Brazil. In: In: South American Symposium on Isotope Geology. https://doi.org/10.1111/j.1365-3121.2011.01023.x/full.

Babinski, M., Boggiani, P.C., Trindade, R.I.F., Fanning, C.M., 2013. Detrital zircon ages and geochronological constraints on the Neoproterozoic Puga diamictites and associated BIFs in the southern Paraguay Belt, Brazil. Gondwana Research 23, 988–997.

Babinski, M., McGee, B., Tokashiki, C.C., Tassinari, C.C.G., Saes, G.S., Pinho, F.E.C., 2018. Comparing two arms of an orogenic belt during Gondwana amalgamation: Age and provenance of the Cuiabá Group, northern Paraguay Belt, Brazil. Journal of South American Earth Sciences 85, 6–42.

Babinski, M. 2011. Geocronologia das glaciações criogenianas do Brasil Central. University of São Paulo, qualified teaching thesis, 182p.

Bandeira, J., McGee, B., Nogueira, A.C.R., Collins, A.S., Trindade, R., 2012. Sedimentological and provenance response to Cambrian closure of the Clymene ocean: The upper Alto Paraguai Group, Paraguay belt, Brazil. Gondwana Research 21, 323–340.

Batalha, R.S., 2017. Estudo de minerais pesados, análise morfológica e datação U-Pb por ICPMS-LA de zircão detrítico - Proveniência dos metassedimentos do Grupo Cuiabá, Faixa Paraguai Norte – MT. Universidade Federal do Mato Grosso, Dissertação de Mestrado, p. 72p.

Boggiani, P.C., Alvarenga, C.J.S. 2004. Faixa Paraguai. In: Mantesso Neto, V.; Bartorelli, A.; Carneiro, C.D.R.; B; Brito Neves, B. (Ed.). Geologia do Continente Sul-Americano. São Paulo: Beca, 2004.

Boggiani, P.C., Coimbra, A.M., 1996. The Corumbá Group (Central South America) in the context of Late Neoproterozoic global changes. Anais Da Academia Brasileira De Ciências. Resumo Das Comunicações 68 (4), 595–596.
Boggiani, P.C., Gaucher, C., Sial, A.N., Babinski, M., Simon, C.M., Riccomini, C., Ferreira, V.P., Fairchild, T.R., 2010. Chemostratigraphy of the Tamengo Formation (Corumba Group, Brazil): A contribution to the calibration of the Ediacaran carbon-isotope curve. Precambrian Research 182, 382–401.
Campanha, G.A.C., Boggiani, P.C., Sallun-Filho, W., Sá, F.S., Zuquim, M.P.S., Piacentini, T., 2011. A Faixa de Dobramento Paraguai na Serra da Bodoquena e Depressão do Rio Miranda. Mato Grosso Do Sul. Revista Do Instituto De Geociências – USP 11 (3), 79–96.
Carneiro, J., Fuck, R., Dantas, E.L., 2021. Arenópolis sequence, evolution of a marginal basin in the Neoproterozoic Goiás magmatic arc, central Brazil. Journal of South American Earth Sciences 106, 103033.
Cawood, P.A., Hawkesworth, C.J., Dhuime, B., 2012. Detrital zircon record and tectonic setting. Geology 40, 875–878.
Chapman, J.B., Ducea, M.N., Kapp, P., Gehrels, G.E., DeCelles, P.G., 2017. Spatial and temporal radiogenic isotopic trends of magmatism in Cordilleran orogens. Gondwana Res. 48, 189–204. https://doi.org/10.1016/j.gr.2017.04.019.
Cordani, U.G., D'Agrella-Filho, M.S., Brito Neves, B.B., Trindade, R.I.F., 2003. Tearing up Rodinia: the Neoproterozoic palaeogeography of South American cratonic fragments. Terra Nova 15, 350–359.
Cordani, U.G., Pimentel, M.M., Ganade de Araújo, C.E., Basei, M.A.S., Fuck, R.A., Girardi, V.A.V., 2013a. Was there an Ediacaran Clymene Ocean in Central South America? American Journal of Science 313, 517–539. https://doi.org/10.2475/06.2013.01.
Cordani, U.G., Pimentel, M.M., Ganade de Araújo, C.E., Fuck, R.A., 2013b. The significance of the Transbrasiliano-Kandi tectonic corridor for the amalgamation of West Gondwana. Brazilian Journal of Geology 43 (3), 583–597.
Cordani, U.G., Ramos, V.A., Fraga, L.M., Cegarra, M., Delgado, I., Souza, K.G., Gomes, F. E.M., Schobbenhaus, C., 2016. Tectonic map of South America. CG-MW-CPRM-SEGEMAR.
Curto, J.B., Vidotti, R.M., Fuck, R.A., Blakely, R.J., Alvarenga, C.J.S., Dantas, E.L., 2014. The tectonic evolution of the Transbrasiliano Lineament in northern Paraná Basin, Brazil, as inferred from aeromagnetic data. Journal Geophysical. Research Solid Earth 119, 1544–1562. https://doi.org/10.1002/2013JB010593.
D'Agrella-Filho, M.S., Cordani, U.G. 2017. The paleomagnetic record of the São Francisco-Congo Craton. In: Heilbron, M., Cordani, U.G., Alkmim, F.F. (eds.) São Francisco Craton, Eastern Brazil, tectonic genealogy of a miniature continente. Springer 16, 305-320. doi: 10.1007/978-3-319-01715-0_16.
Dahlquist, J.A., Verdecchia, S.O., Baldo, E.G., Basei, M.A.S., Alasino, P., Urán, G.A., Rapela, C.W., Campos Neto, M.C., Zandomeni, P.S., 2016. Early Cambrian U-Pb zircon and Hf- isotope data from the Guasayán pluton, Sierras Pameanas, Argentina: implications for the northwestern boundary of the Pampean arc. Andean Geology 43, 137–150.
Dalziel, I.W.D., 1997. Neoproterozoic-Paleozoic Geography and Tectonics: Review, Hypothesis, Environmental Speculation. Geological Society of America Bulletin 109, 16–42.
Dantas, E.L., Alvarenga, C.J.S., Santos, R.V., Pimentel, M.M. 2009. Using Nd isotopes to understand the provenance of sedimentary rocks from a continental margin to a foreland basin in the Neoproterozoic Paraguay Belt, Central Brazil.
DeCelles, G., Giles, K.N., 1996. Foreland basin systems. Basin Research 8, 105–123.
Dorilêo-Leite, A.F.G., Fuck, R.A., Dantas, E.L., Ruiz, A.S., Moniê, P., Iemmolo, A., 2024. Tectonic significance of the late-Ediacaran syn-orogenic basin in the easternmost portion of the Paraguay Belt, Tocantins Province, central Brazil. Precambrian Research 133 (2024), 104735.
Elholou, S., Belousova, E., Griffin, W.L., Peasom, N.J., O'Reilly, S.Y., 2006. Trace element and isotopic composition of GJ red zircon standard by laser ablation. Geochim. Cosmochim. Acta 70 (8), A158.
Escayola, M.P., Pimentel, M.M., Armstrong, R., 2007. Neoproterozoic backarc basin: sensitive high-resolution ion microprobe U-Pb and Sm–Nd isotopic evidence from the Eastern Pampean Ranges, Argentina. Geology 35, 495–498. https://doi.org/10.1130/G23549A.1.
Ferreira, C.O. 2009. A extensão do Arco Magmático de Goiás ao longo do Lineamento Transbrasiliano: Estudo baseado na aplicação dos métodos U-Pb e Lu-Hf por LA-ICP-MS. University of Brasília, Master thesis, 76p.
Frei, R., Døssing, L.N., Gaucher, C., Boggiani, P.C., Frei, K.M., Bech Árting, T., Crowe, S. A., Freitas, B.T. 2017. Extensive oxidative weathering in the aftermath of a late Neoproterozoic glaciation – Evidence from trace element and chromium isotope records in the Urucum district (Jacadigo Group) and Puga iron formations (Mato Grosso do Sul, Brazil): Gondwana Research, v. 49, p. 1–20, doi:10.1016/j.gr.2017.05.003.
Freitas, B.T., Warren, L.V., Boggiani, P.C., Almeida, R.P., Piacentini, T., 2011. Tectono-sedimentary evolution of the Neoproterozoic BIF-bearing Jacadigo Group, SW-Brazil. Sedimentary Geology 238, 48–70. https://doi.org/10.1016/j.sedgeo.2011.04.001.
Freitas, B.T., Rudnitzki, I.D., Morais, L., Campos, M.D.R., Almeida, R.P., Warren, L.V., Boggiani, P.C., Caetano-Filho, S., Bedoya-Rueda, C., Babinski, M., Fairchild, T.R., Trindade, R.I.F., 2021. Cryogenian glaciostatic and eustatic fluctuations and massive Marinoan-related deposition of Fe and Mn in the Urucum District. Brazil. Geology 49 (12), 1478–1483. https://doi.org/10.1130/G49134.1.
Fuck, R.A., Pimentel, M.M., Alvarenga, C.J.S., Dantas, E.L. 2017. The Northern Brasília Belt. In: Heilbron, M., Cordani, U.G., Alkmim, F.F. (eds.) São Francisco Craton, Eastern Brazil, tectonic genealogy of a miniature continent. *Springer,* 11, 205-220. doi: 10.1007/978-3-319-01715-0_11.
Ganade de Araujo, C.E., Rubatto, D., Hermann, J., Cordani, U.G., Caby, R., Basei, M.A.S., 2014. Ediacaran 2,500-km-long synchronous deep continental subduction in the West Gondwana Orogen. Nature Communications 5, 5198.
Geraldes, M.C., Tassinari, C.C.G., Babinski, M., Martinelli, C.D., Iyer, S.S., Barboza, E.S., Pinho, F.E.C., Onoe, A.T., 2008. Isotopic evidence for the late-Brasiliano (500–550 Ma) ore-forming mineralization of the Araés Gold Deposit. Brazil. International Geology Review 50 (2), 177–190.
Godoy, A.M., Pinho, F.E.C., Manzano, J.C., Araújo, L.M.B., Silva, J.A., Figueiredo, M., 2010. Estudos isotópicos das rochas granitoides neoproterozoicas da Faixa de Dobramento Paraguai. Revista Brasileira De Geologia 40 (3), 380–391.
Guimarães, S.B., Moura, M.A., Dantas, E.L., 2012. Petrology and geochronology of the Bom Jardim de Goiás copper deposit (GO). Revista Brasileira De Geociências 42 (4), 841–862.
Hamilton, P.J., O'Nions, R.K., Bridgwater, D., Nutman, A., 1983. Sm-Nd studies of Archaean metasediments and metavolcanics from West Greenland and their implications for the Earth's early history. Earth and Planetary Science Letters 62 (2), 263–272.
Herron, M.M., 1988. Geochemical classification of terrigenous sands and shales from core or log data. Journal of Sedimentary Research 58 (5), 820–829.
Hodel, F., Trindade, R.I.F., Macouin, M., Meira, V.T., Dantas, E.L., Paixão, M.A.P., Rospabé, M., Castro, M.P., Queiroga, G.N., Alkmim, A.R., Lana, C.C., 2019. A Neoproterozoic hyper-extended margin associated with Rodinia's demise and Gondwana's build-up: The Araguaia Belt, central Brazil. Gondwana Research 66, 43–62.
Irvine, T., Baragar, W., 1971. A guide to the chemical classification of the common volcanic rocks. Canadian Journal Earth Sciences 8, 523–548.
Johansson, A., Bingen, B., Huhma, H., Waight, T., Vestergaard, R., Soesoo, A., Skridlaite, G., Krzeminska, E., Schumlyanskyy, L., Holland, M.E., Holm-Denoma, C., Teixeira, W., Faleiros, F.M., Ribeiro, V.R., Jacobs, J., Wang, C., Thomas, R.J., Macey, P.H., Kirkland, C.L., Hartnady, M.I.H., Elington, B.M., Puetz, S.J., Condie, K. C., 2022. A geochronological review of magmatism along the external margin of Columbia and in the Grenville-age orogens forming the core of Rodinia. Precambrian Research 371, 106463.
Julià, J., Assumpção, M., Rocha, M.P., 2008. Deep crustal structure of the Paraná Basin from receiver functions and Rayleigh-wave dispersion: Evidence for a fragmented cratonic root. Journal of Geophysical Research 113, 1–23. https://doi.org/10.1029/2007JB005374.
Laux, J.H., Pimentel, M.M., Dantas, E.L., Armstrong, R., Armele, A., Nilson, A.A., 2004. Mafic magmatism associated with the Goiás magmatic arc in the Anicuns region, Goiás, central Brazil: Sm-Nd isotopoes and new ID-TIMS and SHRIMP U-Pb data. Journal of South American Earth Sciences 16, 599–614.
Leite, A.F.G.D., Sousa, M.Z.A., Ruiz, A.S., Cubas, N., Matos, J.B., Dantas, E.L., Oliveira, J. R., 2018. Petrology and geochronology (U-Pb) of the Caapucú suíte – Southern Paraguay: Post-tectonic magmatism of the Paraguari belt. Journal of South America Earth Sciences 88, 621–641.
López de Luchi, M.G., Dopico, C.I.M., Wemmer, K., Siegesmund, S., 2018. Untangling the Neoproterozoic-Early Paleozoic Tectonic Evolution of the Eastern Sierras Pampeanas Hidden in the Isotopical Record. Book chapter. In, Geology of Southwest Gondwana, pp. 433–466.
Ludwig, K.R., 2008. User's Manual for Isoplot 3.70. Berkeley Geochronol. Center Spec. Publ. 26 (4), 77.
Maniar, P.D., Piccoli, P.M., 1989. Tectonic Discrimination of Granitoids. Geological Society of America Bulletin 101, 635–643.
Manoel, T.N., Selby, D., Galvez, M.E., Leite, J.A.D., Figueiredo, L.N., 2021. A pre-Sturtian depositional age of the lower Paraguay Belt, Western Brazil, and its relationship to western Gondwana magmatism. Gondwana Research 89, 238–246.
Martinelli, C. D. 1998. Petrografia, estrutural e fluidos da mineralização aurífera dos Araés- Nova Xavantina-MT. 1998. Universidade Estadual Paulista. Tese de Doutorado, 183p.
McGee, B., Collins, A.S., Trindade, R.I.F., 2012. G'Day Gondwana – the final accretion of a supercontinent-U-P-b ages from the post-orogenic São Vicente Granite, northern Paraguay Belt, Brazil. Gondwana Research 21, 316–322.
McGee, B., Collins, A.S., Trindade, R.I.F., 2013. A glacially incised canyon in Brazil: further evindece for mid-Ediacaran glaciation? Journal of Geology 121, 275–287.
McGee, B., Collins, A.S., Trindade, R.I.F., Jourdan, F., 2015a. Investigating mid-Ediacaran glaciation and final Gondwana amalgamation using coupled sedimentology and $^{40}Ar/^{39}Ar$ detrital muscovite provenance from the Paraguay Belt, Brazil. Sedimentology 62, 130–154.
McGee, B., Collins, A.S., Trindade, R., Payne, J.P., 2015b. Age and Provenance of the Cryogenian to Cambrian passive margin to foreland basin sequence of the northern Paraguay Belt, Brazil. Geological Society of America, Bulletin 127, 76–86.
McGee, B., Babinski, M., Trindade, R., Collins, A.S., 2018. Tracing final Gondwana assembly: age and provenance of key stratigraphic units in the southern Paraguay Belt, Brazil. Precambrian Research 307, 1–33.
McLennan, S.M., Hemming, S., McDaniel, D.K., Hanson, G.N. 1993. Geochemical approaches to sedimentation, provenance and tectonics. In: Johnsson, M.J., Basu, A., eds. Processes controlling the composition of clastic sediments. Boulder, Colorado. Geological Society of America Special Paper 284, 21-40.
Meschede, M., 1986. A method of discriminating between different types of mid-ocean ridge basalts and continental tholeiites with the Nb-Zr-Y diagram. Chemical Geology 56, 207–218.
Min, A., Hendriks, B., Slejko, F., Comin-Chiaramonti, P., Girardi, V., Ruberti, E., Gomes, C.B., Neder, R.D., Pinho, F.C., 2013. Age of ultramafic high-K rocks from Planalto da Serra (Mato Grosso, Brazil). Journal of South American Earth Sciences 41, 57–64.

Parry, L.A., Boggiani, P.C., Condon, D.J., Garwood, R.J., Leme, J.D.M., McIlroy, D., Brasier, M.D., Trindade, R., Campanha, G.A.C., Pacheco, M.L.A.F., Diniz, C.Q.C., Liu, A.G., 2017. Ichnological evidence for meiofaunal bilaterians from the terminal Ediacaran and earliest Cambrian of Brazil. Nature Ecology & Evolution 1, 1455.

Pearce, J.A., 2008. Geochemical fingerprinting of oceanic basalts with applications to ophiolite classification and the search for Archean oceanic crust. Lithos 100, 14–48.

Pearce, J.A., Stern., R.J. 2006. Origin of back-arc basin magmas: Trace element and isotope perspectives. Geophysical Monograph Series 166, 63-86.

Pearce, J.A., Harris, N.B.W., Tindle, A.G., 1984. Trace element discrimination diagrams for the tectonic interpretation of granitic rocks. Journal of Petrology 25, 956–983.

Pelosi, G.F.F., 2017. Age, Provenance and Tectonic Setting from Southern Portion of the Cuiabá Group: Implications for the Evolution of the Paraguai Belt. Universidade do Mato Grosso, Dissertação de Mestrado, p. 47p.

Piacentini, T., Vasconcelos, P.M., Farley, K.A., 2013. $^{40}Ar/^{39}Ar$ constraints on the age and thermal history of the Urucum Neoproterozoic banded iron-formation, Brazil. Precambrian Research 228, 48–62.

Pimentel, M.M., 2016. The tectonic evolution of the Neoproterozoic Braília belt, central Brazil: a geochronological and isotopic approach. Brazilian Journal of Geology 46, 67–82. https://doi.org/10.1590/2317-4889201620150004.

Pimentel, M.M., Fuck, R.A., 1987. Origem e evolução das rochas metavulcânicas e metaplutônicas da região de Arenópolis (GO). Revista Brasileira De Geologia 17 (1), 2–14.

Pimentel, M.M., Fuck, R.A., 2000. The Neoproterozoic Goiás Magmatic Arc, Central Brazil: A review and new Sm-Nd isotopic data. Revista Brasileira De Geociências 30 (1), 035–039.

Pimentel, M.M., Fuck, R.A., Botelho, N.F., 1999. Granites and the geodynamic history of the Neoproterozoic Brasília Belt, Central Brazil: a review. Lithos 46, 463–483.

Pimentel, M.M., Fuck, R.A., Gioia, S.M.C.L., 2000. The Neoproterozoic Goiás Magmatic Arc, Central Brazil: a review and new Sm-Nd isotopic data. Revista Brasileira De Geociências 30 (1), 35–39.

Pimentel, M.M., Jost, H., Fuck, R.A., Armstrong, R.A., Dantas, E.L., Potrel, A., 2003. Neoproterozoic anatexis of 2.9 Ga old granitoids in the Goiás-Crixás block, Central Brazil: evidence from new SHRIMP U-Pb data and Sm-Nd isotopes. Geologia USP, Série Científica 3, 1–12.

Pinho, F.E.C., 1990. Estudo das rochas encaixantes e veios mineralizados a ouro do Grupo Cuiabá, na região denominada "Garimpo dos Araés" Nova Xavantina. Estado de Mato Grosso. Universidade Federal do Rio Grande do Sul, Dissertação de Mestrado, p. 114p.

Puetz, S.J., Spencer, C.J., Ganade, C.E., 2021. Analyses from a validated global U-Pb detrital zircon database: Enhanced methods for filtering discordant U–Pb zircon analyses and optimizing crystallization age estimates. Earth-Science Rev. 220, 103745 https://doi.org/10.1016/j.earscirev.2021.103745.

Ramos, V.A., Vujovich, G., Martino, R., Otamendi, J., 2010. Pampia: A large cratonic block missing in the Rodinia supercontinent. Journal of Geodynamics 50, 243–255.

Rapalini, A. 2018. A assembly of western gondwana: Reconstruction based on paleomagnetic data. In: S. Siefesmund, M.A.S. Basei, P., Oyhantçabal, S. Oriolo, editors. Geology of Southwest Gondwana, Springer, 3-16.

Rocha, M.P., Schimmel, M., Assumpção, M., 2011. Upper-mantle seismic structure beneath SE and Central Brazil from P- and S-wave regional traveltime tomography. Geophysical Journal International 184, 268–286.

Rocha, M.P., Assumpção, M., Affonso, G.M.P., Azevedo, P.A., Bianchi, M., 2019a. Teleseismic P wave tomography beneath the Pantanal, Paraná, and Chaco-Paraná Basins, SE South America: Delimiting lithospheric blocks of the SW Gondwana Assemblage. Journal of Geophysical Research: Solid Earth 124, 1–18.

Rocha, M.P., Azevedo, P.A., Assumpção, M., Pedrosa-Soares, A.C., Fuck, R., Von Huelsen, M.G., 2019b. Delimiting the Neoproterozoic São Francisco Paleocontinental Block with P-wave traveltime tomography. Geophysical Journal International 2019, 633–644.

Romero, J.A.S., Lafon, J.M., Nogueira, A.C.R., Soares, J.L., 2012. Sr isotope geochemistry and PB-PB Geochronology of the Neoproterozoic cap carbonates, Tangará da Serra, Brazil. International Geology Review 1, 185–203.

Roser, B.P., Korsch, R.J., 1988. Provenance signatures of sandstone-mudstone suítes determined using discriminant function analysis of major-element data. Chemical Geology 67, 119–139.

Schmitt, R.d.S., Fragoso, R.d.A., Collins, A.S. 2018. Suturing Gondwana in the Cambrian: The Orogenic Events of the Final Amalgamation. In: Siegesmund, S., Basei, M., Oyhantçabal, P., Oriolo, S. (eds) Geology of Southwest Gondwana. Regional Geology Reviews. Springer, Cham. https://doi.org/10.1007/978-3-319-68920-3_15.

Schmitt, R., d. S., Costa, R., Collins, A.S., Armistead, S.E. Gomes, I.V., Archibald, D.A., Razakamanana, T. 2021. Tectonic Evolution of an Early Cryogenian Syn-Magmatic Basin in Central Madagascar. Journal of African Earth Sciences. 179, 104205. https://doi.org/10.1016/j.jafrearsci.2021.104205.

Roser, B.P., Korsch, R.J. 1986. Determination of Tectonic Setting of Sandstone-Mudstone Suites Using SiO2 Content and K2O/Na2O Ratio. The Journal of Geology 94, 635–650. https://doi.org/10.1086/629071.

Schwartz, J.J., Gromet, L.P., Miró, R., 2008. Timing and duration of the calc-alkaline arc of the Pampean Orogeny: Implications for the Late Neoproterozoic to Cambrian Evolution of Western Gondwana. The Journal of Geology 116, 39–61.

Seer, H.J., 1987. Litogeoquímica das rochas metavulcânicas do Grupo Bom Jardim de Goiás. In: 1°congresso Brasileiro De Química 1, 299–314.

Seer, H.J., Nilson, A.A. 1985. Contribuições à geologia das unidades pré-cambrianas da região de Bom Jardim de Goiás. In: Simpósio Geológico do Centro-Oeste, 2, ata, SBG-Núcleos Centro-Oeste e Brasília. p. 267-279.

Silva, M.F., 2007. Aerogeofísica, litogeoquímica e geologia na caracterização do rifte intracontinental da Faixa Paraguai. Universidade de Brasília, Dissertação de Mestrado, p. 160p.

Silva, M.F., 2018. Evolução Tectônica de Rift para Margem Passiva da Faixa Paraguai. Universidade de Brasília, Tese de Doutorado, p. 198p.

Sousa, M.F., Silva, C.H., Costa, A.C.D., 2019. Evolução geológica do domínio interno da Faixa Paraguai na Região de Nova Xavantina. Leste De Mato Grosso. Revista Geociências – Unesp 38 (4), 83–851.

Tedeschi, M., Leonardo Rossi Vieira, P., Kuchenbecker, M., Ribeiro, B. V., Barrote, V., Reis, H., Stutenbecker, L., Lana, C., Pedrosa-Soares, A., Dussin, I. 2023. Unravelling the protracted U-Pb zircon geochronological record of high to ultrahigh temperature metamorphic rocks: Implications for provenance investigations. Geosciences. Frontiers 14, 101515. doi:10.1016/j.gsf.2022.101515.

Tohver, E., Trindade, R.I.F., Solum, J.G., Hall, C.M., Riccomini, C., Nogueira, A.C., 2010. Closing the Clymene ocean and bending a Brasiliano belt: Evidence for the Cambrian formation of Gondwana, southeast Amazon craton. Geology 38 (3), 267–270.

Tohver, E., Cawwod, P.A., Rossello, E.A., Jourdan, F., 2012. Closure of the Clymene Ocean and formation of West Gondwana in the Cambrian: Evidence from the Sierras Australes of the southernmost Río de la Plata craton, Argentina. Gondwana Research 21, 394–405.

Tohver, E., D'Agrella Filho, M., Trindade, R.I.F., 2006. Paleomagnetic record of Africa and South America for the 1200–500 Ma interval, and evaluation of Rodinia and Gondwana assemblies. Precambrian Research 147, 193–222. https://doi.org/10.1016/j.precamres.2006.01.015.

Tohver, E., D'Agrella-Filho, M.A., Trindade, R.I.F., 2016. Paleomagnetic record of Africa and South America for 1200–500 Ma interval, and evaluation of Rodinia and Gondwana assemblies. Precambrian Research 147, 193–222.

Tokashiki, C.C., Saes, G.S., 2008. Revisão estratigráfica e faciologia do Grupo Cuiabá no alinhamento Cangas-Poconé, baixada Cuiabana. Mato Grosso. Revista Brasileira De Geociências 38 (4), 661–675.

Trindade, R.I.F., D'Agrella-Filho, M.S., Epof, I., Brito Neves, B.B., 2006. Paleomagnetism of Early Cambrian Itabaiana mafic dikes (NE Brazil) and the final assembly of Gondwana. Earth and Planetary Science Letters 244, 361–377.

Valeriano, C.M. 2017. The Southern Brasília Belt. In: Heilbron, M., Cordani, U.G., Alkmim, F.F. (Ed.). São Francisco Craton, Eastern Brazil, tectonic genealogy of a miniature continent. Springer, 189-204. doi: 10.1007/978-3-319-01715-0_10.

VanDecar, J.C., James, D.E., Assumpção, M., 1995. Seismic evidence for a fossil plume beneath South America and implications for plate driving forces. Nature 378, 25–31.

Vasconcelos, B.R. 2018. Proveniência sedimentar do Grupo Cuiabá na Faixa Paraguai Meridional. Universidade de Brasília. PhD thesis, 172p.

Vermeesch, P., 2012. On the visualization of detrital age distributions. Chemical Geology 312–313, 190–194. https://doi.org/10.1016/j.chemgeo.2012.04.021.

Vermeesch, P., 2018. IsoplotR: A free and open toolbox for geochronology. Geosciences Frontiers 9, 1479–1493. https://doi.org/10.1016/j.gsf.2018.04.001.

Viehmann, S., Bau, M., Buhn, B., Dantas, E.L., Andrade, F.R.D., Walde, D.H.G., 2016. Geochemical characterisation of Neoproterozoic marine habitats: Evidence from trace elements and Nd isotopes in the Urucum iron and manganese formations, Brazil. Precambrian Research 282, 74–96.